Solar System Observations with JWST

James Norwood
New Mexico State University

Heidi Hammel
Association of Universities for Research in Astronomy

Stefanie Milam
Goddard Space Flight Center

John Stansberry
Space Telescope Science Institute

Jonathan Lunine
Cornell University

Nancy Chanover
New Mexico State University

Dean Hines
Space Telescope Science Institute

George Sonneborn
Goddard Space Flight Center

Matthew Tiscareno
Cornell University

Michael Brown
California Institute of Technology

Pierre Ferruit
ESA / ESTEC

This version is also available at arXiv:1403.6845v1 [March 24, 2014].

Contents

Abstract

The James Webb Space Telescope will enable a wealth of new scientific investigations in the near- and mid-infrared, with sensitivity and spatial/spectral resolution greatly surpassing its predecessors. In this paper, we focus upon Solar System science facilitated by JWST, discussing the most current information available concerning JWST instrument properties and observing techniques relevant to planetary science. We also present numerous example observing scenarios for a wide variety of Solar System targets to illustrate the potential of JWST science to the Solar System community. This paper updates and supersedes the Solar System white paper published by the JWST Project in 2010 (Lunine et al., 2010). It is based both on that paper and on a workshop held at the annual meeting of the Division for Planetary Sciences in Reno, NV in 2012.

Introduction

The James Webb Space Telescope (JWST) will succeed the Hubble Space Telescope as NASA's premier space-based telescope for planetary science and astrophysics. This 6.5-meter telescope, which is optimized for observations in the near- and mid-infrared portions of the electromagnetic spectrum, will be equipped with four state-of-the-art imaging, spectroscopic, and coronagraphic instruments. These instruments, along with the telescope's moving target capabilities, will enable the study of a vast array of Solar System objects with unprecedented detail, unhindered by the telluric features that afflict ground-based observers.

The intent of this white paper is to provide the latest information regarding JWST instrument sensitivities and capabilities for planetary science applications. We also present a number of hypothetical Solar System observations as a means of demonstrating potential planetary science observing scenarios, although the list of applications discussed here is far from comprehensive. The goal of disseminating this updated information is to stimulate discussion and participation among members of the planetary science community, many of whom are expected to become eventual users of JWST, and to encourage feedback on any desired capabilities that would enhance the usage of JWST for Solar System observations.

The number of possible types of Solar System observations has grown with further consideration by the JWST Science Working Group, by the increased participation of the community through workshops, and by the successful implementation of the moving target tracking. For this reason, we do not attempt an encyclopedic survey of all possible targets and observational types, but rather consider exemplary types of observations that demonstrate the substantial capability of the observatory in furthering Solar System research. It is our hope that readers will be sufficiently stimulated by the examples herein that they will develop their own proposals that might be submitted under general observing time.

Motivation for planetary science observations with JWST

Numerous planetary science investigations will be enabled with JWST. The near- and mid-infrared spectral coverage and sensitivity afforded by JWST complements NASA's other Solar System exploration platforms such as Earth-based telescope facilities—both ground-based and in Earth orbit—and interplanetary spacecraft that continue to explore the Solar System through orbiter, flyby, and lander/rover missions. When JWST joins these important components of NASA's planetary exploration portfolio, it will offer improvements in sensitivity, spatial resolution, spectral resolution and coverage, and/or geographic area of exploration. JWST will contribute to the overarching objectives of planetary science, namely to understand planet formation, evolution, and the suitability of planets as habitats, through high-fidelity infrared imaging and spectroscopy of both large and small bodies in the Solar System.

The suite of Solar System observations that will be enabled by JWST will advance our understanding of our own planetary system as well as more general astrophysical processes such as planet formation and evolution.

Furthermore, if recent history is any indication, the number of known exoplanetary systems will continue to grow rapidly in the future, along with our ability to characterize exoplanets. Our own Solar System serves as a benchmark against which all other planetary systems are compared, and the insights gained into the physical processes governing the formation and evolution of our own system are by extension also relevant to the burgeoning field of exoplanet science. For example, the same dynamical processes manifest in the atmospheres of the giant planets of our own Solar System through cloud motions and signatures of trace molecular species are likely at work in extrasolar giant planet atmospheres. The study of hydrological, carbon dioxide, and methane cycles of our terrestrial planets and Titan will yield important insights into what we might expect to observe once the quest for Earth-like exoplanets transitions from discovery to characterization. The analysis of small bodies in our Solar System, which provide a window to the early stages of planetesimal formation from the protosolar nebula, will provide clues to the general formation processes occurring in stellar disks throughout our galaxy. In summary, there are numerous investigations of Solar System targets that can be enabled through JWST observations. These studies will not only advance our understanding of planetary formation, evolution, and habitats, but will also inform future exoplanetary investigations of sister worlds that have only recently been discovered.

Special needs for Solar System observations

Capabilities for Solar System observations

Observations of various Solar System bodies can be conducted with JWST, and the science working group has put forth a significant effort in establishing the capabilities of the observatory for moving targets and bright objects. As the instruments are delivered and characterized, more accurate assessments of their capabilities are being made and will be updated through commissioning.

Moving target capability

JWST is designed to observe Solar System objects having apparent rates of motion up to 30 milliarcseconds/second. This capability includes the planets, satellites, asteroids, trans-Neptunian objects, and comets beyond Earth's orbit (see Table 1). Solar System targets can be observed over the full range of JWST's field of regard (solar elongation of 85° to 135°, and a roll range of ±5° about the telescope's optical axis). The size of the field of regard is dictated by the thermal design of the observatory, specifically the 21 m × 14 m sunshield. By keeping the telescope and instruments in always the sunshield's shadow they are passively cooled to $T \sim 40$ K.

During the observation of a moving target, the science target is held fixed in the desired science aperture by controlling the guide star to follow the inverse of the target's trajectory. The ground system and on-board pointing control software use polynomial ephemerides for the target generated by JPL's HORIZONS system. The JWST guider field of view (2.2′ × 2.2′) is located in the telescope focal plane several arcminutes from the science apertures. The pointing stability specification for moving target observations is 0.050″ (3σ).

Table 1. Movement rates of various Solar System targets.

Object	Minimum rate (mas/sec)	Maximum rate (mas/sec)
Mars	0.485	28.27
Ceres	0.152	11.81
Jupiter	0.019	4.48
Saturn	0.016	1.74
Uranus	0.012	1.09
Neptune	0.020	0.74
Pluto	0.004	0.65
Haumea	0.372	0.62
Eris	0.058	0.30

Event-driven operations

On-board software scripts autonomously control the execution of the JWST science timeline (Balzano and Zak 2006). An *Observation* is a series of exposures with a single instrument to achieve a science objective. A *Visit* is a series of exposures obtained with one science instrument and a single guide star (within the $2.2' \times 2.2'$ field of the guider). An *Observation* may be split into more than one *Visit* (the *Visit* is basic unit of scheduling) depending on its duration, distribution of guide stars, and other factors. The scripts respond to actual slew completion or on-board command execution, making operations more efficient. Scripts also respond to an interrupted or a failed *Visit*, moving on to the next valid *Visit*. *Visits* are scheduled with overlapping windows to provide execution flexibility and to avoid lost time. Each visit has an *Earliest Start Time*, a *Latest Start Time*, and a *Latest End Time* that define when each visit can be scheduled and executed. These timing parameters are determined from the program's scientific objectives. For visits without specific constraints on when they must execute, the interval between *Earliest* and *Latest Start Times* is expected to be a significant fraction of a day.

An observing plan covering about ten days will be uplinked weekly, but plan updates could be more frequent if necessary (for example, to accommodate a Target of Opportunity (TOO) observation). Event-driven operations are expected to increase observing efficiency by at least 10%, relative to fixed-time scheduling.

The event-driven operations system supports time-critical observations and TOOs. The minimum response time for TOOs is 48 hours (observation approval to execution). The JWST scheduling system easily accommodates observations with critical timing requirements. For such visits, the *Earliest* and *Latest Start Times* are set to be very close together, forcing the visit to be scheduled and executed in the time interval defined by the observer. These capabilities are needed by a wide range of science programs, not just Solar System science.

Brightness Limits

The observed brightness of light reflected from a Solar System object is directly proportional to the area of the telescope's mirror and the angular size and albedo of the object, and inversely proportional to the square of the distance of the object from observer and the Sun. At thermal wavelengths the same is true except that the brightness depends on the object's temperature which scales as $(1\text{-}A)^{0.25}$, where A is the bolometric albedo. The high sensitivity and large aperture of JWST are ideal for the smaller Solar System bodies such as KBOs and distant comets. In contrast, the outer Solar System planets are extremely bright, limiting the observatory's capabilities for conducting observations on these targets. Venus and Mercury cannot be observed due to the solar elongation limits on JWST's pointing (limited from 85° to 135°). Below we present a few cases where outer-planet observations are feasible based on preliminary knowledge of observatory and instrument performance; however, this is not inclusive of all Solar System studies that can be conducted, and special cases (modes, target acquisition, etc.) may exist for some extreme targets. Where there is disagreement, results presented in this study supersede those in the JWST technical report by Meixner et al. 2008 (JWST-STScI-001375).

Table 2. Estimated surface brightness (Jy/□″) of outer planets and Pluto.

Planet	Heliocentric Dist. (AU)	Radius (km)	albedo	2 μm (Jy/□″)	4-5μm	10-12 μm	Diam. (″)	Area (□″)
Mars	1.67	3397	0.2	100	34	2800	7.0	39
Jupiter	5.2	71492	0.52	22	100	35	39	1172
Saturn	9.5	60268	0.47	6.0	2	10	18	243
Uranus	19.2	25559	0.51	1.6	0.47	0.3	3.7	11
Neptune	30.1	24766	0.41	0.5	0.16	100	2.3	4
Pluto	33.0	1150	0.55	5.5 mJy	1.6	0.3	0.10	0.008

Notes: These values are the sum of reflected solar flux and thermal emission. Jupiter's surface brightness is for a Jovian "hot spot," which is brighter than the disk average. Pluto's brightness is for full disk, not surface brightness. Angular sizes assume each target is at a solar elongation of 90°, and therefore within the JWST field of regard. Mars is assumed to be near aphelion, when it is at its dimmest.

The four JWST science instruments provide imaging, coronagraphy, and spectroscopy over the 0.6–28.5 μm wavelength range. (See Gardner et al. (2006) for instrument design details.) Imaging fields of view are ~2′ × 2′, with pixel sizes of 0.032″ (0.6-2.5 μm), 0.065″ (2.5-5 μm), and 0.11″ (5-28.5 μm). The spectroscopic capabilities include 1-5 μm multi-object spectroscopy over 3′ × 3′ with 250,000 individually addressable shutters (each 0.2″ × 0.46″), integral field spectroscopy covering 1-28.5 μm with a field of view of 3″ × 3″ or larger, and several long slits. The spectrographs provide spectral resolving powers of ~100 to ~2700 over the 1-28.5 μm range.

NIRCam

The minimum time to read out a NIRCam detector in full-frame mode is 10.74 seconds. Mars, Jupiter, and Saturn will saturate in all NIRCam filters in full-frame mode, and Uranus and Neptune will saturate at the shorter wavelengths. Subarray performance in this application, e.g. against a bright extended source, has not been confirmed. Assuming that this mode works satisfactorily, subarrays will provide significantly shorter integration

times, and make it possible to observe these objects without saturating the detectors. Figure 1 illustrates the configuration of subarrays in the NIRCam short wavelength (SW) channel (0.6-2.5 μm) for imaging of extended sources. Gaps between the four detectors in the SW focal plane would be filled by dithering. The longwave (LW) channel has a single detector with a plate-scale twice that in the SW channel, and is automatically configured such that the LW FOV is matched to the footprint of all 4 SW FOVs. With 640×640 pixel subarrays the FOV is 41.6″ across, large enough to encompass the disk of Jupiter, as shown in Figure 1.

The 1-5 μm spectra of the outer planets are compared with the NIRCam saturation limits (for 640^2 subarrays) in Figure 2. Uranus and Neptune can be observed in all NIRCam filters without saturating. Jupiter and Saturn exceed the saturation limits shortward of about 1.5 μm, although it may be possible to observe them using the medium bandwidth filters F140M and longer; in the longwave channel they can be observed in many of the filters without saturating. Because its apparent size is about half that of Jupiter, Saturn could be observed using the 320^2 subarray configuration (with saturation limits four times higher); that would probably allow for un-saturated images in all NIRCam filters. Mars is so bright that it can only be observed in the narrow-band filters except at 4.3 μm. The 320^2 subarray doesn't increase the saturation limits enough to change that, but Mars is small enough to nearly fit within a 160^2 subarray, where the saturation limit is 16 times greater than shown in Figure 2. The 160^2 subarray is available in point-source photometry mode, and by executing dithers with a throw of a few arcseconds the entire disk could quickly be mapped.

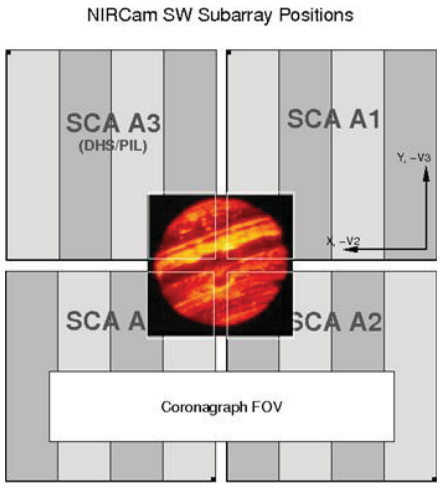

Figure 1. Proposed configuration for observing bright targets with NIRCam.

Jupiter (and most of the bright objects in the Solar System) can be observed if the object is centered between the 4 detectors allowing for four subarrays with a 40″ FOV (see Figure 1) across both the short wavelength and long wavelength channels (Figure 2).

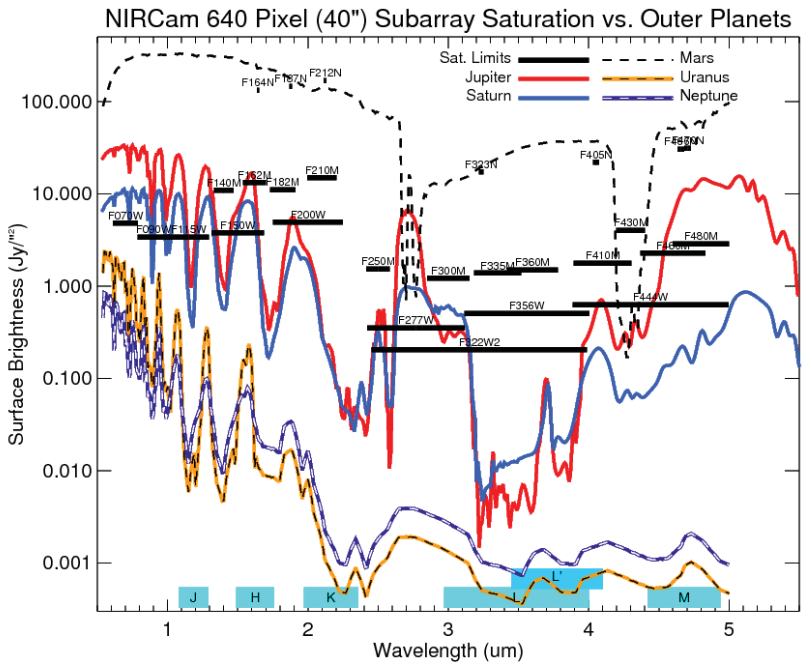

Figure 2. Saturation limits (black) for the NIRCam filters employing the subarray configuration in Figure 1, compared to planetary spectra.

NIRSpec

The full-well capacity for the NIRSpec detectors is close to 80,000 electrons. Brightness limits for NIRSpec observations of the bright Solar System bodies were derived using our current knowledge of the instrument. Two different modes were considered: the IFU mode where a 3″ × 3″ field of view is observed with a sampling of 0.1″, and the 0.2″ × 3.3″ fixed-slit mode. These were then compared to each planet's surface brightness (Table 2) for various configurations and resolving powers. The results are summarized in Figures 3-4 and Table 3.

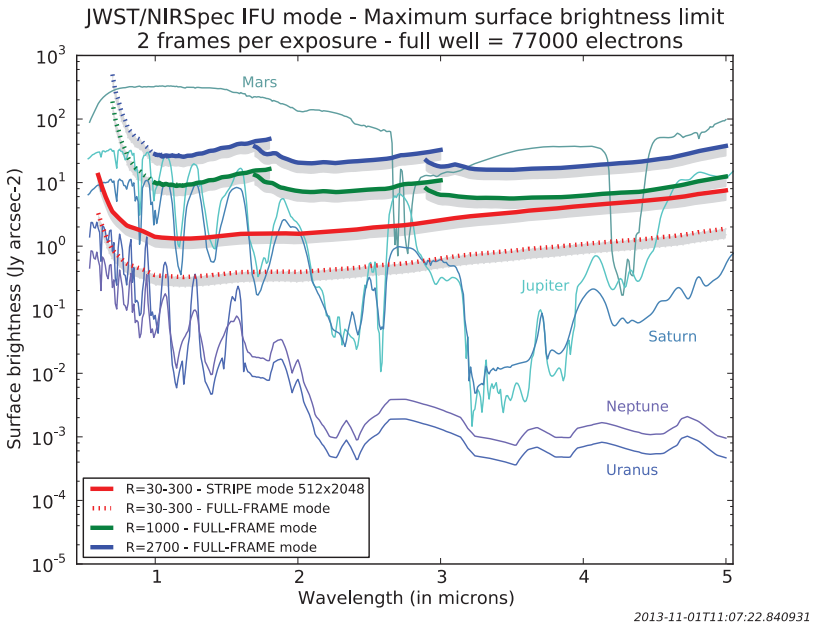

Figure 3. Maximum surface brightness limits for NIRSpec in IFU mode. The gray zone below each curve highlights the range corresponding to a (not unrealistic) 30% uncertainty level on the limits. The planet spectra are the same as in Figure 2.

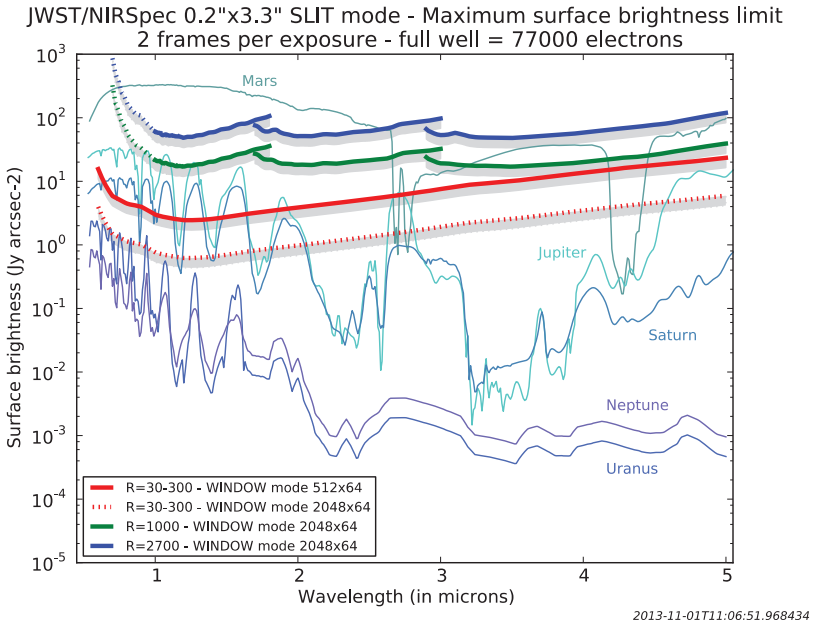

Figure 4. Maximum surface brightness limits for NIRSpec in slit mode. The gray zone below each curve highlights the range corresponding to a (not unrealistic) 30% uncertainty level on the limits. The planet spectra are the same as in Figure 2.

Table 3. Targets observable with NIRSpec.

Planets	Available modes	Comments
Mars	At short wavelengths: 0.2″ × 3.3″ slit at the highest spectral resolution and with non-standard short windows (shorter wavelength coverage). At long wavelengths: 0.2″ × 3.3″ slit at the highest spectral resolution and with a standard window.	At the limit of what can be done with NIRSpec.
Jupiter	At short wavelengths: 0.2″ × 3.3″ slit at the highest spectral resolution and with a standard window. More options available at long wavelengths where lower spectral resolutions become available with the 0.2″ × 3.3″ slit and where high spectral resolution observations in IFU mode become possible.	Observable with the IFU at long wavelengths.
Saturn	Most spectral resolutions are now available when using the 0.2″ × 3.3″ slit with standard windows. Observable with the IFU at high spectral resolution and possibly at medium spectral resolution (will depend on the actual performances of the instrument).	
Uranus, Neptune, and Pluto	The IFU becomes the preferred mode here and all spectral resolutions become progressively available as the surface brightness of the planet decreases.	The apparent size of the planet becomes a good match to the IFU field of view.

MIRI

The MIRI instrument has nine broad-band imaging filters (with four defined subarrays, plus full field, to date), a medium-resolution spectrometer (MRS), and a low-resolution spectrometer (LRS). For bright extended objects, the SUB64 subarray (frame time of 0.066 s)[1] is the most promising approach for imaging. However, the performance of subarrays on bright sources has not yet been verified. If the capability to use subarrays on bright sources is confirmed in future tests, and assuming a full well depth[2] of 225,000 e^- and a quantum efficiency midway between the specification and 100% (e.g., 70% at 5.6 μm, 80% around 12 μm, 75% around 20 μm), an estimate of the integration time to saturation can be made for each of the surface brightnesses presented in Table 2. In this SUB64 imaging mode, all the bright planets except Mars can be observed with at least one of the broad-band MIRI imaging

[1] Two frames minimum are required to fit the slope and derive a count rate, so the minimum on-source integration time is 0.132 seconds.

[2] Note that the surface brightnesses presented in Table 2 are disk-averaged. In practice, planets may have varying features across the disk, so conservatively using an upper limit to the integration time of ~2/3 full-well may be more appropriate.

filters (see Chen et al. 2010; JWST-STScI-001757). The MIRI spectrometers offer more options for observations since they disperse the light of bright sources. Again, all the bright planets are accessible in at least half the available mid-infrared spectroscopic bandwidth except Mars.

NIRISS

The NIRISS instrument has a larger pixel resolution than NIRCam, higher sensitivity to extended emission < 2.5 μm than NIRCam (but at lower spatial resolution). NIRISS can image with a full 2048×2048 pixel array, SUB256, SUB128 and SUB64 with readout times of 10.74 s, 0.70 s, 0.18 s, and 0.05 s, respectively, including seven wide filters and five medium filters. Currently, imaging is only offered from the full array since NIRCam will likely provide better performance in the subarray modes. Spectroscopy with NIRISS will be accessible with either the GR150 grism or the GR700 grism. The GR150 offers Wide-Field Slitless Spectroscopy with a resolving power of ~150 and spectral coverage of 0.8-2.2 μm. Sensitivity limits for this mode are presented in the specific examples to follow and allow for spectral observations of most objects in the solar system at a lower spectral resolution. The GR700 grism supports the Single-Object Slitless Spectroscopy (SOSS), cross-dispersed orders, with resolving power of 300-800 and spectral range of 0.6-2.5 μm with up to three orders. This would allow synoptic observations across this entire wavelength range; good for surface variation analysis or even early characterization of distant comets or other small, bright isolated sources due to effectively spreading flux in the cross-dispersion direction by about 35 pixels. Finally, NIRISS offers a unique mode of Aperture Masking Interferometery with NRM. This is a seven-hole aperature mask with 21 distinct baselines. While this mode was optimized for exoplanet detections around bright stars, case studies are being considered for solar system targets, such as binary asteroids.

Example observing programs

Mars

Studies of Mars with JWST offer the promise of unique and important new contributions to Mars science and to NASA's future mission goals. Specifically, global-scale near-IR observations can: (1) determine the variability of major and secondary atmospheric species like CO_2, CO, and H_2O, providing data for photochemical and dynamical modeling of the present Martian climate; (2) constrain the near-IR radiative and absorptive properties of airborne dust, another key component of the present Martian climate system; (3) help to quantify the surface volatile budget and resource potential by detecting and mapping the distribution of H_2O-bearing or OH-bearing surface minerals like clays and hydrates; and (4) assess the magnitude and scale of diurnal, seasonal, and interannual volatile transport through direct near-IR detection and discrimination of surface and atmospheric H_2O and CO_2 ices/clouds, especially in the polar regions.

The orbital eccentricity of Mars (e = 0.0933) means that the insolation between perihelion and aphelion varies by ~40%, so any attempt to use seasonal symmetries is not a viable strategy for understanding seasonal transitions (e.g., spring equinox vs. fall equinox does not represent the same transition). In addition, these seasonal transitions are out of phase with opposition, so observations must be obtained at multiple epochs and over extended, contiguous periods. Current and planned probes are not capable of sampling multiple local times (i.e., local diurnal variation) on sub-seasonal time-scales for most of the Martian surface area; they are not Mars-synchronous, and are positioned in high-inclination orbits. Furthermore, there are no planned thermal-IR instruments for Mars.

While HST affords a look at the entire disk, the current instrumentation is limited to wavelengths shorter than 2 μm. In addition, the orbital constraints on HST forbid prolonged, continuous monitoring of the atmospheric changes over a Martian day. JWST solves these problems with its suite of instruments, and its L2 orbit, which enables the observatory to monitor the Martian atmosphere on timescales from a few minutes to weeks, with any cadence that is required by the observer.

While Mars would saturate in MIRI observations, example observations with NIRSpec (0.6-5 μm) include synoptic monitoring of gases, aerosols, and dust in the Martian atmosphere over the entire disk. NIRSpec will be used to measure the strengths of ice features, which constrain particle size (aerosol components). Due to the high surface brightness of Mars, observations of this planet with NIRSpec will only be possible beyond 2.5 μm and using the 0.2″ × 3.3″ slit at high spectral resolution (see Figure 4). The primary atmospheric components measurable with NIRSpec are CO and H_2O. NIRSpec would only be able to detect methane in concentrations about a factor of 5-10 larger than previous estimates and newer upper limits (e.g., Webster et al. 2013).

Observations would be conducted over two consecutive Martian days (24.6 Earth hours), four times during the Martian year. The four yearly epochs will coincide with important seasonal transitions where the atmosphere is undergoing significant heat load changes. It is necessary to monitor Mars for two full Martian days in order to get full coverage of the Martian surface. This observation program also assumes Mars to be near aphelion to reduce the planet's brightness.

Jupiter and Saturn

The JWST era will be an important time period for extending, enhancing, and complementing the infrared observations of Jupiter and Saturn made in the preceding decades by Galileo, Cassini, Juno, New Horizons, Spitzer, and HST. Jupiter is the largest, most massive, and closest of the gas giant planets, and thus has been the best studied with both ground-based and space-based (orbiter and flyby) assets. Cassini is the longest orbiting mission in the outer Solar System, and has been observing many aspects of the Saturn system for nearly the past decade. Despite these observational achievements, there are numerous outstanding questions about the giant planet atmospheres that can be addressed with JWST.

The relationships between heat transport, atmospheric dynamics, and chemical processes are fundamental to our understanding of the giant planet atmospheres. Furthermore, Jupiter represents the archetype of a broad class of giant planets, many of which are now known to exist in orbit around other stars, and provides a nearby "laboratory" where we can test our understanding of giant planet formation and evolution. Two example outstanding questions in the field of giant planet atmospheres, which are relevant to both our own gas giants as well as a myriad of exoplanets, include

- How does atmospheric circulation detected at the cloud tops relate to deeper atmospheric motions and heat transport from the interior? and
- What is the link between atmospheric dynamics, chemistry, and cloud microphysics?

Many components of these questions can be addressed with JWST observations of Jupiter and Saturn. The infrared spectra of Jupiter and Saturn are shaped by a combination of reflected sunlight and thermal radiation escaping from the deeper atmosphere, modulated by the spectral properties of the gases and aerosols present in the overlying cloud decks. For example, the relationship between atmospheric chemistry and dynamics can be explored through the observation of disequilibrium species such as phosphine (PH_3) and arsine (AsH_3), and the spatial variations thereof. These species are tracers of tropospheric mixing since their observed abundances exceed those predicted from thermochemical equilibrium calculations. The chemical composition of giant planet atmospheres as well as cloud and aerosol properties can be determined using IR imaging and spectroscopy from JWST, as detailed below.

NIRCam Imaging

The near-IR spectra of Jupiter and Saturn are dominated by methane absorption bands. When imaged in these bands, the planets appear dark, thus any reflective aerosols must be located high enough in the atmospheres to be above most of the methane-absorbing gas. Imaging in these bands therefore provides an opportunity to sound the upper troposphere or lower stratosphere and gain information about the variation of certain atmospheric properties (e.g. wind speeds) as a function of altitude. As shown in Figure 2, the NIRCam filters in which images of Jupiter and Saturn may be obtained include F140M, F164N, F182M, F187N, F200W (Saturn only), F210M, F212N, F250M, F300M, F323N, F335M, F356W, F360M, F405N, F410M, F430M, F444W (Saturn only), F460M (Saturn only), F465N, F470N, and F480M (Saturn only). This assumes a 640×640 pixel (40″ × 40″) subarray in the 2.5-5 μm channel, with the subarrays configured so that they are positioned on the four corners of the individual detectors as shown in Figure 1.

Near-IR images of Jupiter and Saturn are shown in Figure 5. This spectral region covers a wide range of physical processes, including gaseous and aerosol absorption and scattering, thermal radiation, and cloud opacity. JWST will enable extensive imaging of the gas giant planets through filters that are sensitive to species such as ammonia and methane, providing insight into energy transport and the chemistry in these atmospheres.

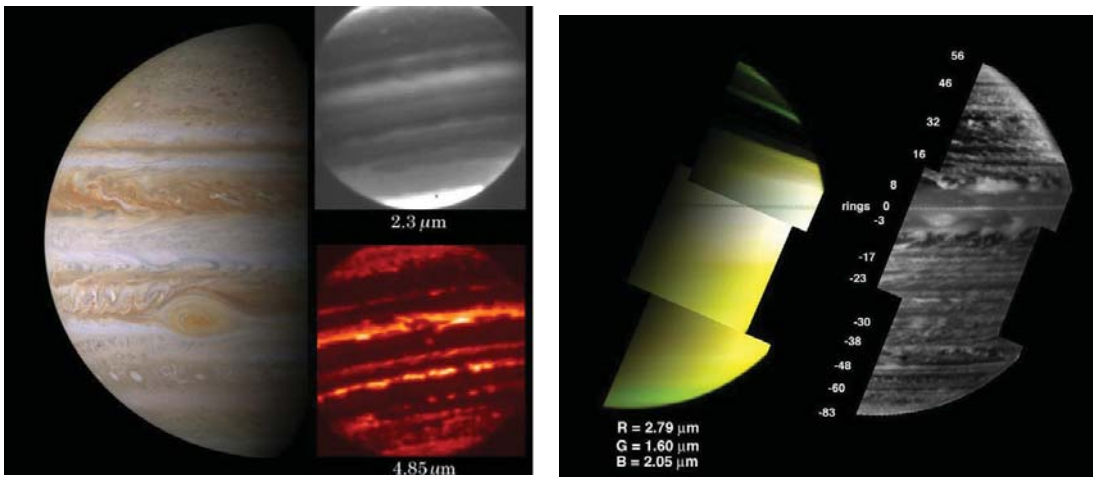

Figure 5. Left Panel: Jupiter's visible cloud deck is shown in the left image, taken by the ISS imager on the Cassini spacecraft in December 2000. The upper right image shows a ground-based image of Jupiter taken from NASA's Infrared Telescope Facility (IRTF) through a 2.3 μm filter, which is centered on a strong methane absorption band. The white clouds in this image are higher than the darker regions. The bottom right image shows an IRTF image of Jupiter at 4.85 μm, which is sensitive to thermal radiation from the lower cloud layers. In this image dark regions correspond to thicker clouds, whereas bright areas are relatively cloud-free. Right Panel: Saturn images taken by the Visual and Infrared Mapping Spectrometer (VIMS) on board the Cassini spacecraft. The left image shows a color composite sensitive to aerosols in Saturn's upper atmosphere, and the right image shows Saturn at 4.85 μm. Both images are from Sanchez-Lavega (2011), *An Introduction to Planetary Atmospheres*, Chapter 5.

NIRSpec Spectroscopy

As described in Table 4, both Jupiter and Saturn can be observed with NIRSpec in fixed-slit mode (with a slit size of 0.2″ × 3.3″) or IFU mode (with a field of view of 3″ × 3″), and resolving powers of ~1000 and 2700. The 1-5 μm

spectral region in the gas giants is quite rich, containing absorptions due to gaseous ammonia and methane, pressure-induced molecular hydrogen absorption, and disequilibrium species such as phosphine, arsine, and carbon monoxide (Figure 6). JWST will enable targeted spectroscopy of localized regions on Jupiter and Saturn, covering for example Jupiter's Great Red Spot or a storm cloud on Saturn, which will provide unique data concerning the linkage between local chemistry in the gas giant atmospheres and larger scale atmospheric dynamics.

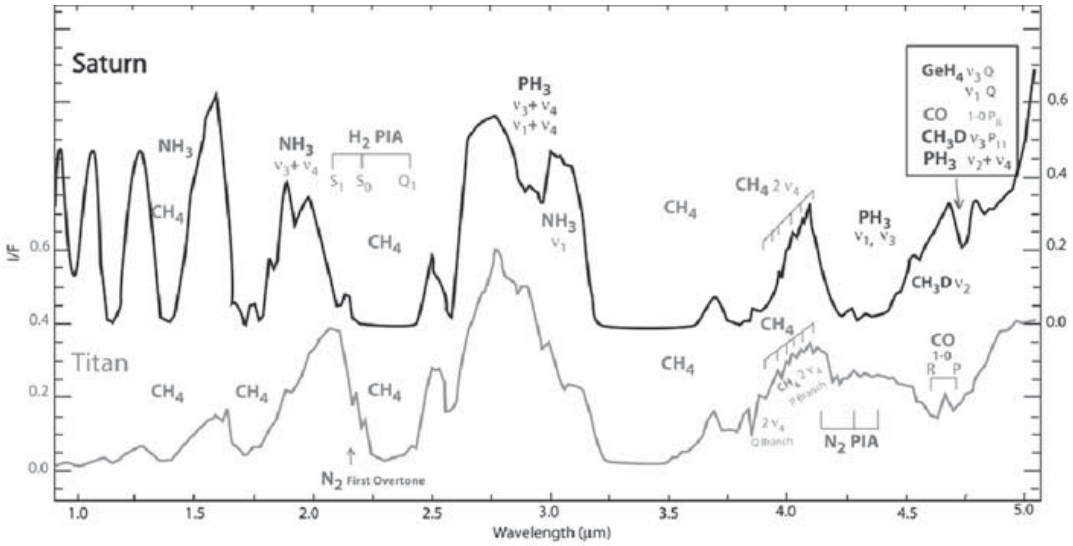

Figure 6. VIMS spectrum of Saturn (darker line) over a spectral region comparable to that of NIRSpec. The spectral resolution of the VIMS data is ~200; NIRSpec will be able to match or exceed this, providing a more detailed understanding of the chemistry and dynamics in the giant planet atmospheres. Figure from Baines et al. (2005).

MIRI Imaging

As mentioned above, for bright extended sources such as the giant planets, imaging with MIRI is best accomplished in the SUB64 subarray mode, which yields a field-of-view size of 7″. Thus, in order to image the entire disk of either Jupiter or Saturn, multiple pointings will be required to create a full-disk mosaic. Figure 7 illustrates the surface brightness of Jupiter and Saturn along with the saturation limits of the MIRI filters. The Jupiter curves include both a hot spot, where the ammonia cloud deck is relatively thin, allowing one to see to regions in the planet dominated by Jupiter's thermal emission; and a zone, where the ammonia clouds are thicker and block the Jovian blackbody radiation. Jupiter's hot spots will likely be too bright for all the MIRI filters with the possible exception of F560W; the zones on Jupiter will be visible in the F560W filter as well as perhaps the F770W filter. Saturn will be observable in all MIRI filters shortward of 17 μm (i.e. F560W, F770W, F1000W, F1130W, F1280W, and F1500W).

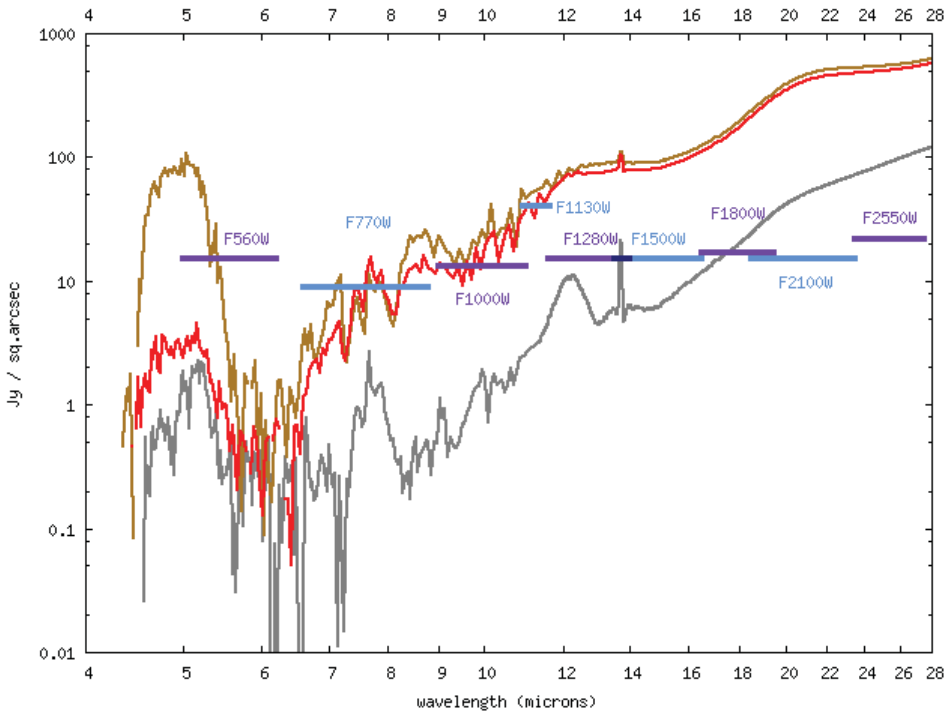

Figure 7. Spectra of a Jovian hot spot (brown), a Jovian zone (red), and Saturn (grey) (G. Bjoraker, personal communication), compared to saturation limits of MIRI filters assuming SUB64 sub-array viewing with minimum integration time.

MIRI Spectroscopy

Spectra of the giant planets can be acquired with MIRI in several integral field unit (IFU) medium resolution spectroscopy modes shortward of 10 μm. As shown in Figure 7, the IR spectra of the gas giants are shaped by gaseous absorption and emission features such as that due to acetylene (C_2H_2) near 14 μm. The MIRI IFU's are significantly smaller than the angular sizes of Jupiter and Saturn (~3″ vs. ~20-40″), so they can be used for targeted observations of latitudes of particular interest, such as polar regions with stratospheric haze, convective cloud regions, and vortices such as the Great Red Spot.

Uranus and Neptune

The ice giants Uranus and Neptune are much more distant than Jupiter and Saturn, and as a result it has been a greater challenge to observe them in detail. It was not until the debut of space telescopes and adaptive optics that Earth-based observations were finally able to resolve individual features on these two planets, such as latitudinal banding and isolated cloud features. In addition to serving as one of the few facilities with the spatial resolution for such observations, JWST will provide substantial improvements over existing capabilities. It has a larger collecting area than Hubble and Spitzer, allowing a greater signal-to-noise ratio in its observations; and it will expand spectral coverage into the mid-infrared, a region unavailable to Hubble and Keck.

Most features in the near-IR spectra of Uranus and Neptune arise from variability in the absorption spectrum of methane. The absorption strength of methane varies by several orders of magnitude, allowing observations to probe a wide variety of altitudes. In spectral regions where multiple CH_4 lines overlap for strong absorption, we see only light scattered at high altitude, primarily from stratospheric haze. On the other hand, in the windows with minimal CH_4 absorption, we see down to the upper cloud decks, understood to be placed between 1 and 10 bars. The precise altitudes of these cloud layers may be determined from spectral regions where CH_4 absorption is of intermediate strength, such as at the boundaries of the CH_4 windows. Furthermore, examination of different CH_4 windows will reveal properties of the clouds themselves: for example, as the wavelength increases beyond the size of a typical cloud particle, the cloud's ability to effectively scatter sunlight decreases.

In the mid-IR, the reflectance spectra for these planets are replaced by thermal emission. In this spectral region the dominant opacity source is collisional absorption between H_2 and He. Also present are numerous emission features due to CH_4, CH_3D, and higher-order hydrocarbons created through high-altitude photochemistry. Mid-IR observations with JWST can greatly improve our understanding of these planets' thermal structure, D/H ratio, and photochemical processes.

While most ground-based studies of Uranus and Neptune have been limited to full-disk observations, the high spatial resolution of JWST enables observation of how the features described above vary across the face of each planet. Knowing how the cloud layers, hydrocarbon distribution, and other properties change with latitude and longitude will greatly assist in the development of dynamical models that characterize these planets' atmospheric circulation. Repeated observations will provide temporal information as well. In addition to greatly improving our state of knowledge of Uranus and Neptune, such investigations will also be useful in comparative planetology, illuminating the properties that make the ice giants a unique class of planet, distinguishing them from the gas giants Jupiter and Saturn.

NIRCam Imaging

For observing the outer planets and other bright compact objects, sub-array imaging has been developed for NIRCam and MIRI in order to lessen the minimum integration time. NIRCam's pixel scales are 0.032″ between 0.6 and 2.3 μm, and 0.065″ between 2.4 and 5.0 μm: Uranus' diameter in these modes would be 112 and 55 pixels, while Neptune would be 72 and 35 pixels across.

For reflected-sunlight spectra, Uranus and Neptune are observable with all NIRCam filters, as the planets' surface brightnesses are $\lesssim$0.5 times the saturation limits. Useful NIRCam filters include F182M, which spans the boundaries of windows in the absorption spectrum of methane; F335M, which covers an H_3^+ feature at 3.4 μm; and F480M, which catches a CO feature at 4.7 microns. Numerous features also span boundaries of methane absorption windows, allowing identification of vertical structure. At longer wavelengths, the planets' cloud decks become more optically thin, enabling views deeper within their atmospheres.

NIRSpec Spectroscopy

NIRSpec is capable of observing Uranus and Neptune from 0.6 to 5.0 microns at various spectral resolutions (R ~100, 1000 and 2700). The most interesting option is to use the IFU to observe these planets. In this mode, a total of 900 spectra can be obtained simultaneously, covering a 3″ × 3″ field of view, with spatial sampling of 0.1″. Uranus' angular diameter of 3.6″ will be larger than the IFU's field of view, but full coverage may be obtained with mosaicing. An observer may also achieve better spatial resolution by dithering observations.

MIRI Imaging

As discussed in an earlier section, MIRI will best observe Uranus and Neptune using a 64 × 64 sub-array, which has a field of view 7″ across, twice Uranus' angular diameter. Shown in Figure 8 are the surface brightnesses of Uranus and Neptune compared to the saturation limits using the SUB64 sub-array. Neptune will be observable using the F560W, F1000W, and F1130W filters. Uranus, being dimmer, will be visible in all these filters except F2100W and F2550W.

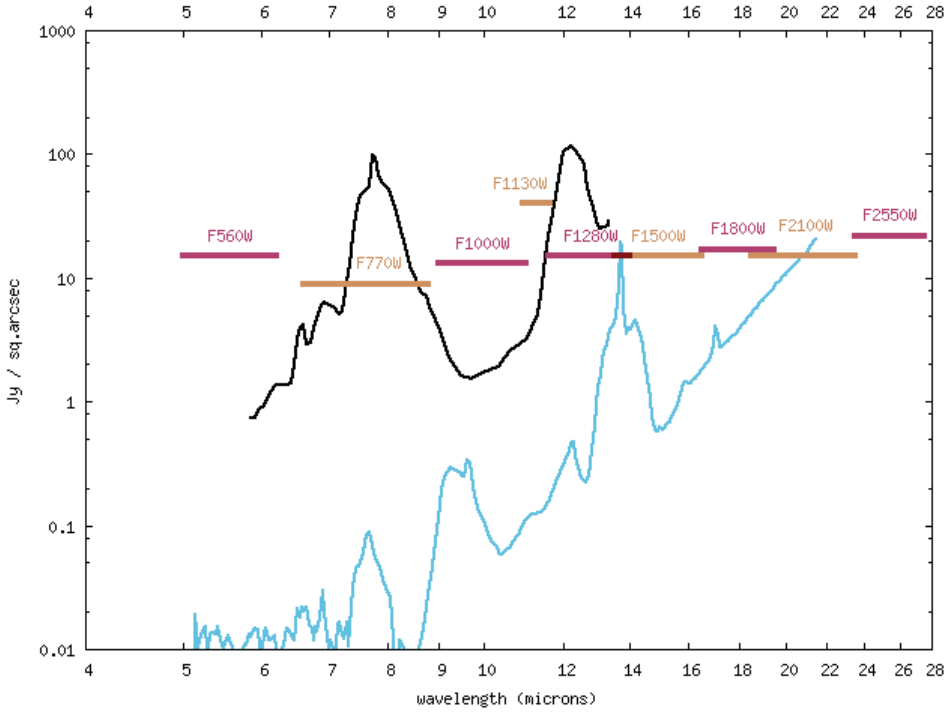

Figure 8. Spectra of Neptune (black; Fletcher et al. 2010) and Uranus (blue; Orton, Glenn [2011], personal communication), compared to saturation limits of MIRI filters assuming SUB64 sub-array viewing with minimum integration time.

MIRI Spectroscopy

MIRI's Medium-Resolution Spectrograph (MRS) has four square integral field units that are able to provide spatially resolved spectra across Uranus and Neptune, as shown in Figure 9. For example, the shortest-wavelength unit has a field of view 3.7″ on a side, which is divided into 30 strips for spectra. Including the pixel scale of the spectra, the IFU effectively divides the field into 0.18″ × 0.19″ regions: about twenty across the Uranian disk, and 12 across the Neptunian disk. The longer-wavelength IFU's have lower spatial resolution, with the poorest still offering 13 × 5.5 resolution elements across Uranus, and 8.5 × 3.5 across Neptune. This spatial resolution may be improved by a factor of 2 with four-position dithering.

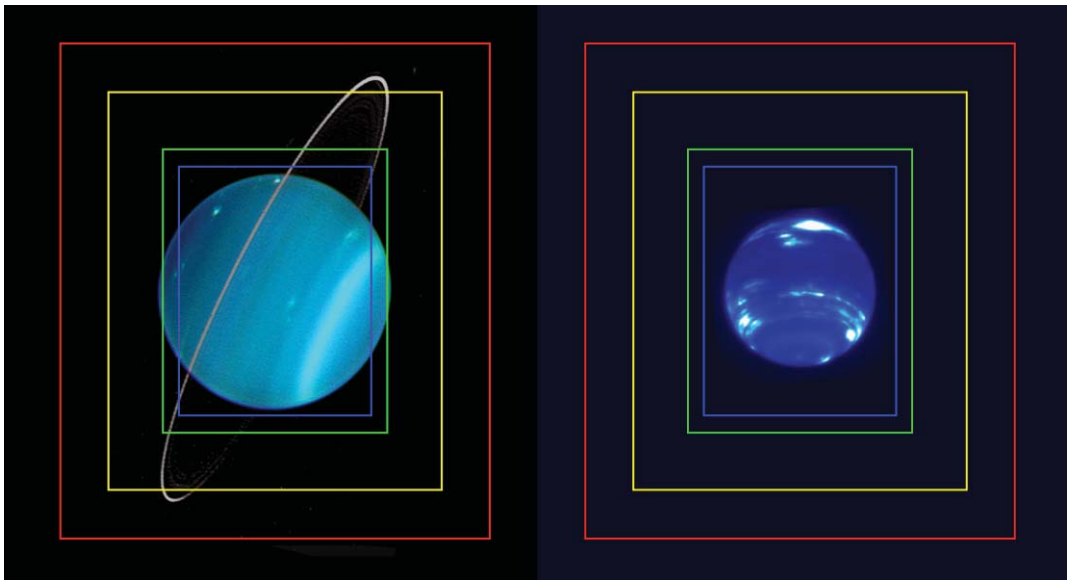

Figure 9: Sample viewing geometry for observing Uranus and Neptune with the Medium-Resolution Spectrograph IFUs. Shown are the fields of view for the four different IFUs compared to the typical sizes and orientations of Uranus and Neptune during JWST operations. Uranus image credit: L. Sromovsky and W. M. Keck Observatory; Neptune image credit: I. de Pater, H. B. Hammel, and W. M. Keck Observatory.

Europa

Jupiter's satellite Europa contains what is likely the largest reservoir of accessible liquid water anywhere in the Solar System other than the Earth itself (Pappalardo et al. 1998). With energy input from a warm radioactively decaying chondritic-composition core and an intense external radiation environment, chemical reactions in the internal ocean might be capable of building some of the pre-biotic materials thought to be necessary for life (Hand et al. 2007). But even after almost a decade of intense scrutiny from the Galileo spacecraft, debate still persists about the nature of the surface chemistry and the relative roles of exogenous radiation processing versus endogenous oceanic emplacement. From the current data, Europa can be viewed as a purely passive ice shell onto which ion and electron bombardment creates a limited chemical cycle confined to a thin surface layer, or it can be seen as a geologically active body with a chemically rich ocean and a sulfur-rich surface, both of which feed each other and record a complex chemical cycle.

The key to determining the nature of Europa is the composition of the surface and whether or not chemicals expected from an oceanic source can be seen on the satellite. The surface of the trailing side of Europa, in particular, is dominated by some sort of hydrated compound, rather than more pure water ice seen on the leading side, but the precise composition of this dominant chemical component on the trailing side of Europa is still unresolved. Much of the reason for the chemical uncertainty is the spectral similarity of many of the proposed constituents, particularly in the well-observed 1-2.5 μm range where spectra of hydrated materials are dominated by the strong absorptions due to their water components and the lack of diagnostic spectral features out to 5 μm observed by the Galileo spacecraft.

Europa and the other icy Galilean satellites are poorly characterized beyond 5 μm, and in particular between 5 and 15 μm where Voyager obtained few results. This spectral region contains anion-specific combination bands of proposed constituents of the icy satellite surfaces, key spectral features that are diagnostic of the radiolytic cycle, and the potential for unexpected discoveries.

On Europa, many of the most important potential spectral features lie in the 5-10 μm region. A series of MIRI spectra covering this wavelength range and sampling ~4 regions around the satellite would allow several key scientific investigations, including:

1. **Searching for the strong spectral signature of hydrated minerals** (Figure 10). If the surface of the trailing side of Europa is rich in ocean-derived hydrated minerals, their spectral signature could dominate the 5-7 μm region. Radiolytic-produced sulfuric acid, in contrast, is essentially featureless in this spectral range. Spectral differences between the leading water ice rich hemisphere and the trailing hydrate rich hemisphere could be particularly illuminating. The clear detection of hydrated minerals would demonstrate a strong connection between the interior ocean and surface, and point to a rich chemistry in the interior and on the surface of Europa.

2. **Understanding the importance of a radiolytic carbon cycle.** To date, it is known that water and sulfur participate in the radiolytic cycle, but no evidence for carbon-based radiolysis has been found in spite of the presence of CO_2 in the surface ices of Europa (Carlson et al. 2009). Laboratory experiments (Figure 11) have shown strong carbonic acid features at 5.83 μm, 6.63 μm, and 7.65 μm when simulated Europa ices are bombarded with electrons (Gerakines et al., 2000; Hand et al., 2007). If Europa's surface is rich in carbonic acid and has an active ice shell that exchanges material with the ocean, then Europa's ocean might not only be oxygen-rich (Chyba, 2000), but it could be alkaline and contain a biologically useful source of carbon (Hand et. al., 2007).

3. **Searching for carbonyls (C=O) and amides (H-N-C).** These may be detected by observing the broad 6-7 μm water ice feature, whose shape is modified by these species (Figure 11). Nitrogen in particular, has never been detected at Europa and could be an important unexplored component of the satellite's current ocean or surface chemistry.

4. **Searching for possible organic features (C-C, C-H, C=C) in the 6-8 μm region**. Organics have been detected on Ganymede and Callisto in the 3.44-μm C-H region (McCord et al., 1998), but to date no organics have been observed on Europa. Laboratory experiments show that under Europan conditions, the radiolytic processing of hydrocarbons produces distinct absorptions in the 6-8 μm range (Hand and Carlson, 2011). In particular, methane is produced and trapped in the ice. Recent results in the 3.44-μm region with Keck spectroscopy (Brown and Hand, in prep) suggest that detection of organics is unlikely; nonetheless, the importance of organic chemistry warrants a search for these features on Europa.

5. **Detection of unexpected spectral features.** While laboratory experiments have attempted to simulate all of the relevant chemistry on Europa, much remains unknown. The discovery of any new features could be indicative of a major chemical pathway previously unknown on Europa and the other satellites.

For a bright object as well-studied as Europa, few opportunities exist to observe completely unseen spectral regions. It is thus no surprise that a first look at this spectral region could potentially yield so rich a bounty. Accomplishment of any one of the scientific objectives here has the chance of achieving a major breakthrough in our understanding of the chemistry of Europa and its relationship with an interior ocean.

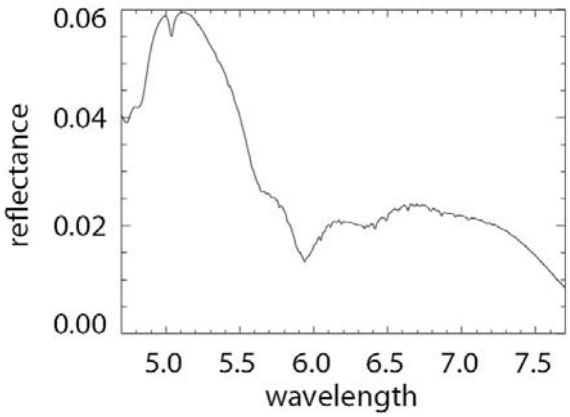

Figure 10. Reflectance spectrum of bloedite ($Na_2Mg(SO_4)_2 \cdot 4H_2O$), an evaporite that is an example of types of hydrated minerals proposed for the surface of Europa. The distinctive spectral features seen on bloedite are typical of these sorts of evaporates. Sulfuric acid, in contrast, is featureless at these wavelengths.

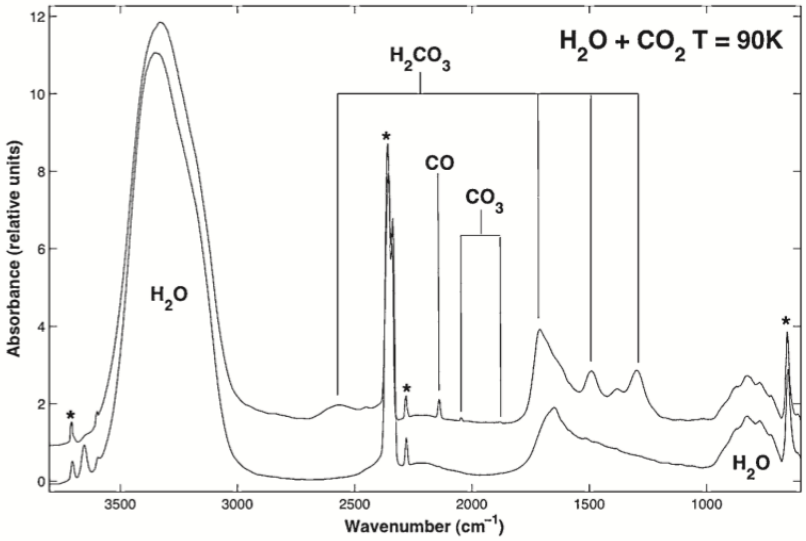

Figure 11. Spectra of H_2O and CO_2 ice before (bottom) and after (top) irradiation. Production of carbonic acid (H_2CO_3) can be detected by the strong absorption lines beyond 5 μm (wavenumber smaller than 2000 cm^{-1}) . Such features on Europa would be a clear indication of an active radiolytic carbon cycle and the beginning of the formation of more complex hydrocarbons. From Hand et al. (2007).

Titan

Titan is a target of the very highest astrobiological interest in our own solar system. It is the second largest moon in the Solar System, has a nitrogen atmosphere several times denser at its surface than that of the Earth at sea level, and boasts an active equivalent of the Earth's hydrological cycle in which two hydrocarbons—methane and ethane—take the place of water, each cycling on different timescales (Lunine and Lorenz, 2009; Aharonson et al. 2009).

Titan is richly endowed in organic molecules on the surface; a series of lakes and seas at polar latitudes hold more hydrocarbon material than the known oil reserves on the Earth (Lorenz et al., 2008). Its nitrogen-methane atmosphere, by virtue of continuous loss of hydrogen liberated from photolyzed methane in the upper atmosphere, is not strongly reducing, and hence is comparable to the pre-biotic Earth's atmosphere in net redox propensity for synthesizing organic polymers. While the chemistry of the atmosphere is well known, that of the surface is not. However, the atmospheric chemistry liberates hydrogen from methane to create a suite of higher carbon-number hydrocarbons and nitriles, whose fate in the extraordinarily cold atmosphere (94 K at the equatorial surface, 90 K at the poles) must be to condense and fall to the surface. Some of this material falls directly into the lakes and seas or is transported there by winds; other aerosols agglomerate to form sand-sized particles comprising the equatorial dunes.

Impacts melt the water ice crust and internally-generated volcanism might as well, leading to locations on the surface where the organics react with water over significant timescales to produce amino and carboxylic acids, as well as other precursors to biomolecules. Thus, while the low temperatures rule out continuous surface liquid water and hence life, Titan is a Mercury-sized world upon which some of the steps associated with the prebiotic synthesis of polymers essential to life are played out—over and over again with every impact.

The US-European mission Cassini-Huygens entered Saturn orbit in 2004 to begin an exploration that continues beyond the four-year prime mission into the "equinox mission" (2008-2010) (referring to the seasonal phase of Saturn and Titan) and the current "solstice mission" (2010-2017), after which it will be directed into a destructive entry of Saturn's atmosphere to avoid contaminating Titan or Enceladus. In 2005 the instrumented Huygens probe descended through the atmosphere to the surface, relaying images of valley networks evidently carved by liquid methane. In total the mission has told us that organic deposits are indeed widespread across the surface, and hints of variations in the organic composition can be seen in the medium-resolution (R ~ 150 at 2 μm) near-infrared spectroscopy performed by Cassini.

However, gaps will remain in our knowledge when final observations of Titan by Cassini are made in 2017. These gaps are the result of several limitations of Cassini. First, geometric constraints associated with the fixed-pallet placement of instruments on the Cassini orbiter (a compromise due to cost) dictate that each of the close flybys will be devoted to only a subset of the instrument techniques. In the end, radar will cover only 40% of the surface at its best spatial resolutions of hundreds of meters. Second, the VIMS near-infrared spectrometer has a lower spectral resolution and sensitivity compared to JWST. The limited spectral resolution is particularly frustrating because Titan's atmosphere must be viewed through a scattering haze of photochemical aerosols and at wavelengths in between the deep absorbing atmospheric methane bands. The VIMS wavelength bands are such that residual methane absorption remains a problem, and atmospheric models must be used to remove this residuum. Finally, there was no possibility for Cassini to cover a full Titan year, 29.5 Earth years. Because of the axial tilt of Titan (essentially coaligned with the spin axis of Saturn), Titan experiences seasonal shifts of sunlight similar in amplitude to that of the Earth. Spacecraft missions to date, and those planned, will cover a portion of Titan's year corresponding to northern late fall through the first "day" of northern summer. JWST's period of operation is unique in that it will cover the portion of Titan's year corresponding to all but the very earliest part of the northern summer.

HST and adaptive-optics ground-based telescopes have achieved diffraction-limited imaging of Titan from Earth. HST NICMOS observations of Titan demonstrated spatial resolution of roughly 200-300 km resolution near the Titan equator and sufficient signal-to-noise to identify the darkest areas as having near-infrared albedos consistent with hydrocarbons (Meier et al., 2000). Ground-based telescopic studies can do what Cassini cannot: provide frequent if not continuous coverage of changes in the atmosphere and on the surface. Ground-based observations suggested short-term changes in the 1-2 μm region of the spectrum associated with the formation of clouds even prior to Cassini (Griffith, 2000). In 2008 a major outburst of mid-latitude clouds was observed from the IRTF

(Schaller et al., 2009), and in 2010 Cassini observed a major outburst of equatorial clouds, with the surface darkening for weeks thereafter interpreted to be soil damp from methane rain (Turtle et al. 2011).

By 2017 we will be left with the following questions:

1. What does the surface look like in higher-resolution (R ~ 3000 vs. 200) near-IR spectroscopy?
2. What time-variable phenomena might occur due to seasonal (decadal) variations or stochastic surface events in the near-infrared and in that part of the mid-infrared (640 cm^{-1}) where the atmosphere is once again optically thin enough to see the surface?

JWST can make NIRCam images, and NIRSpec IFU spectral imaging of Titan to build on the 2004-2017 Cassini mission survey, creating a potentially long (10 year +) baseline of spaceborne near-infrared observations of Titan's surface and atmosphere during a seasonal configuration hitherto unexplored in the infrared. The pixel size on NIRCam gives about the same spatial resolution on Titan as Hubble (Table 2), but the signal-to-noise is much higher. Spectral resolution a factor of 6 better than on Cassini can be accomplished using the NIRSpec, allowing for spectra far more diagnostic of the types of organic species present on the surface. Thus while Cassini gets better spatial resolution, JWST will achieve higher spectral resolution with useful spatial resolution (as shown in Figure 12) over the mid-latitude regions of Titan. Of interest is whether surface changes or secular atmospheric changes are in evidence over a decadal timescale. With NIRSpec, the ability to probe the atmosphere over several levels down to the surface provides a unique long-term capability that is unavailable from Hubble and will cease to be available from Cassini after 2017. Thus JWST provides long-time baseline continuity throughout the infrared.

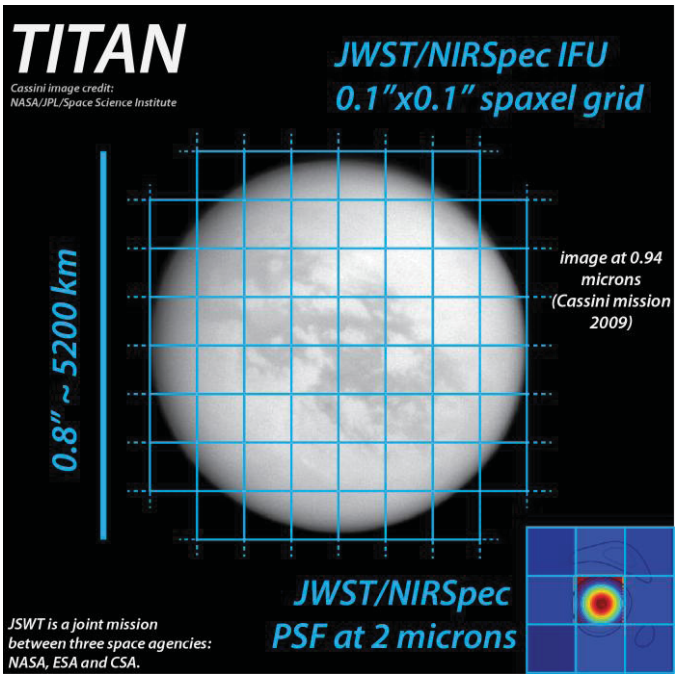

Figure 12. Example of the spatial coverage provided by the NIRSpec IFU on Titan.

One approach is to take NIRCam, NIRSpec and MIRI data on Titan over three equally spaced intervals during the 16-day orbit of Titan, which is phase-locked to Saturn. This provides images and spectra centered approximately 120º apart from each other, and hence global coverage. Cloud movement in the stratosphere, based on our

understanding of Titan's winds, occurs with a velocity of 100 m/sec and hence it requires many hours to track cloud movement in detail. Cloud tracking with HST was very difficult because of the telescope's 90-minute orbit around the Earth; with JWST at L2 it will be much easier. Beyond the initial cloud campaign, revisits to Titan once per year should be done to map in imaging and spectroscopy each of the hemispheres to look for longer-term changes.

Of additional interest is whether surface changes or secular atmospheric changes are in evidence over a decadal timescale. The year 2009 corresponded to the onset of northern hemisphere spring equinox, and the polar regions where large numbers of lakes and one Caspian-sized sea are present experienced sunlight for the first time in almost 15 years. Dramatic changes are expected in the atmosphere above the lakes region and on the surface itself. JWST will be able to monitor these changes beginning a year after the end of the Cassini mission in 2017.

Other icy satellites

The satellite systems of the giant planets are host to great diversity as well as insight into such topics as volatile transport, low-temperature chemistry, and the history of the Solar System. With JWST, these bodies may be studied with unprecedented detail. The satellites' surfaces display prominent near-infrared ice signatures that NIRSpec can observe with high spectral resolution. In the mid-infrared, the thermal properties of these objects may be studied with MIRI observations with greater signal-to-noise than Spitzer. The superior collecting area of JWST will also facilitate observations of smaller objects, enabling near- and mid-infrared spectroscopy of most outer irregular satellites for the first time.

Examples of icy-satellite projects possible with JWST observations include

- Investigation of longitudinal (and possibly latitudinal) variations in surface composition, particularly ices. This may benefit models of inter-satellite relations (such as sputtering from Phoebe's surface being related to Iapetus' varied surface [Tamayo et al. 2011]) and models of volatile transport on individual satellites. Seasonal effects may also be determined.

- Characterization of surface ices to determine their physical state, relative abundances (e.g., CO_2 vs. H_2O), and chemical evolution. For example, the properties of the surface ices may address the degree to which irradiation plays a role in their physical/chemical state, as seen in the "Pac-Man" features on Mimas and Tethys (Howett et al. 2012).

- Analysis of the chemical composition of tiny satellites to determine their origin, particularly through comparison with ring material and comets. Any identifiable differences among the satellites may indicate contrasting histories.

- Using mid-infrared observations to constrain the internal heat levels of satellites, which will benefit models of orbital migration. Such observations may also determine whether Miranda and Ariel are active (or were in the recent past) (Pappalardo and Schubert 2013; Castillo-Rogez and Turtle 2012), and whether Triton may support a subsurface ocean (Gaeman et al. 2012).

While the Cassini mission has explored the Saturnian satellites in the near- and mid-infrared with high spatial resolution, there are ways JWST observations can improve this dataset. NIRSpec offers a greater spectral resolution (R = 2700) compared to VIMS (R ~ 200), allowing better identification and characterization of key absorption features. JWST will also fill the gap between 5 and 7 μm not covered by VIMS and CIRS. Furthermore, JWST will extend the temporal baseline of these satellite observations, extending the seasonal coverage of the Saturnian system through the approach to southern solstice.

For most satellites, observations at the four cardinal points in the orbit are desired to obtain coverage of the sub-planet, anti-planet, leading, and trailing hemispheres. For most principal satellites, it is possible to acquire spectra at all four positions within a single epoch; the only such satellites with orbital periods longer than ~20 days are Iapetus

(79 days) and Phoebe (1.5 years). Seasonal considerations will be important in planning such observations as different latitudes enter or leave view. This will be particularly important for the satellites of Uranus and Neptune due to their long seasonal cycles. Certain latitudes of Uranian satellites will only be visible at the start of the JWST mission (as Uranus will be approaching its 2030 solstice), while certain latitudes in the Neptunian system will only be visible at the end of the mission (in the approach to equinox in 2038). Effects due to seasonal changes in the insolation pattern may be monitored as well, particularly for active bodies like Enceladus and Triton, and for satellites whose activity is unknown (such as Ariel).

Multiple-Satellite Spectroscopy

In addition to standard individual observations of satellites, simultaneous spectroscopy of multiple satellites is possible with NIRSpec's microshutter assembly (MSA). While tracking on the central planet (or on background stars) for an extended period of time, shutters are held open in anticipation of satellites passing through, as shown in Figure 13. Spectra from multiple adjacent slits may be combined in cases where a satellite crosses multiple apertures, and/or where the satellite in question is larger than the size of an aperture. With this method, one hour of observation may result in numerous several-minute spectra totaling ~1 hour or more. This scenario is more efficient than the standard method of observing satellites one by one, because less time is required for system procedures. (Note that data processing associated with these observations will have to take into account the fact that the satellites will not be present in their apertures for the full integration.)

Observing with this method works best with the inner satellites of Uranus and Neptune, due to their faster orbital motion and the lack of a bright ring system (although issues with Saturn's rings will be minimized during the planet's 2025 equinox). Outer large satellites, having slower angular speed, tend to linger in the same aperture long enough to saturate; tracking on background stars while the planet exhibits greater angular speed may counter this effect, at the expense of losing inner-satellite spectra due to interference from the planet itself or other satellites. Outer irregular satellites tend to be spaced farther apart than is feasible for NIRSpec's field of view.

Satellite Discovery and Astrometry

Observations with JWST will be particularly useful in efforts to discover new satellites. While the available field of view is too small for initial investigations, the telescope's large collecting area will be particularly valuable in follow-up observations of potential targets identified by large-scale surveys. Since most outer irregular satellites are expected to have low albedos, observing their mid-infrared thermal radiation is ideal for such observations. However, since the background signal (largely zodiacal light) also becomes brighter in this spectral region, the optimal MIRI filter varies depending on the satellite's expected temperature. Estimates of the minimum satellite sizes detectable with MIRI imaging are given in Table 4.

Among the confirmed satellites, some small satellites have orbits that are chaotic or otherwise not well constrained: particularly Saturn's moons Prometheus and Pandora (Farmer and Goldreich 2006), and Uranus' moon Mab (Kumar et al. 2011). Earth-based monitoring of such satellites has been difficult due to their small sizes. Given JWST's great sensitivity to faint objects, JWST observations will greatly contribute to these satellites' astrometric data sets.

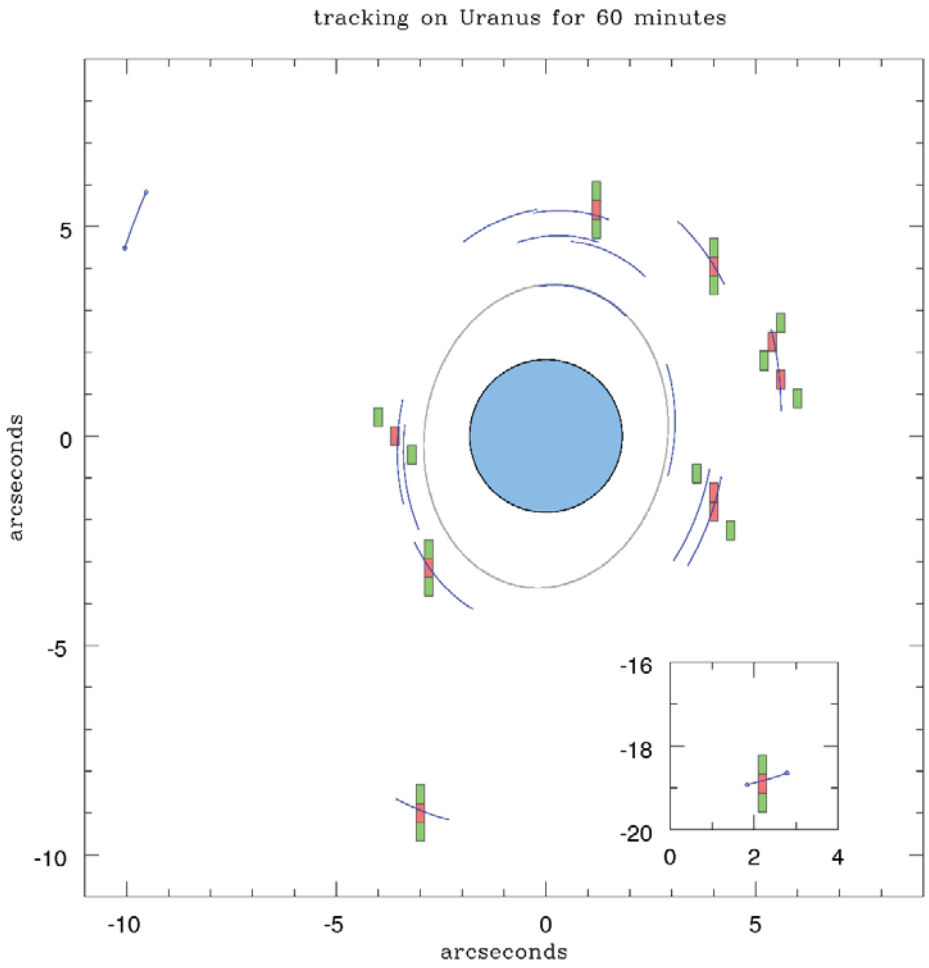

Figure 13. An example MSA configuration for observing the inner Uranian system for one hour, at a randomly chosen time on September 28, 2020 (a valid time for observing Uranus with JWST). Uranus is shown at center, with the Epsilon Ring in gray. Open apertures are shown as colored rectangles: red for apertures that will result in object spectra, and green for nearby "empty" spectra to use for calibration. Observed satellites include (from top to bottom) Cupid, Puck, Mab (with two apertures), Cressida, Perdita (with two apertures), Desdemona, Miranda, and Umbriel (inset). Ariel, at left, is unobservable in this arrangement as it will saturate. The shortest-timespan spectrum will be that of Cupid, at 6.8 minutes. This scenario will produce satellite spectra totalling 2.1 hours.

Planet	Optimal Filter	Satellite diameter (km)
Jupiter	F1500W	0.3
Saturn	F1500W	1.5
Uranus	F2100W	9
Neptune	F2550W	30

Table 4. Estimated minimum sizes of satellites observable with SNR=10 after 10,000 seconds of integration. The satellites are assumed to follow the Standard Thermal Model, with low albedos such that $(1-a)^{1/4} \approx 1$. Background signal was estimated using the Exposure Time Calculator, assuming maximum zodiacal light brightness. Due to the gradually changing nature of a satellite's predicted brightness relative to the background, filters adjacent to the optimal filter will provide similar results.

Rings

The rings that adorn the four giant planets are of prime importance as accessible natural laboratories for disk processes, as clues to the origin and evolution of planetary systems, and as shapers as well as detectors of their planetary environments (Tiscareno, 2013). The retinue of small moons accompanying all known ring systems is intimately connected as both sources and products, as well as shepherds and perturbers, of the rings.

Imaging of faint objects

In the context of rings, observations of faint targets are complicated by the nearby presence of the bright planet. Strategies are needed to enhance the apparent brightness of desired targets and/or to suppress the apparent brightness of the planet. JWST will be equipped with filters that allow it to image giant planet systems at wavelength bands in which the planet is greatly darkened by atmospheric absorption due to methane and other atmospheric constituents. For observations of faint moons or rings that are close to bright giant planets, this will lead to greatly improved signal-to-noise and spatial resolution comparable to HST and other observatories operating in the same wavelength bands. (Put another way, JWST will operate within the infrared methane bands at a spatial resolution comparable to that at which HST operates in visible bands, with vastly improved signal-to-noise when suppression of glare from the planet is an important factor.) As a result, JWST will provide major advances in resolving and separating the main rings of Uranus and Neptune, improving upon HST and ground-based observations of their fine structure (de Pater et al., 2005, 2006, 2007; Showalter and Lissauer, 2006).

JWST will have new sensitivity to yet-undiscovered faint rings, including the predicted rings of Mars (Showalter et al., 2006) and Pluto (Steffl and Stern, 2007). The New Horizons spacecraft, whose flyby of Pluto will pre-date JWST, will likely not have the last word on Pluto's possible rings due to its flyby speed and limited range of viewing geometries. JWST will be ideal for follow-up observations, possibly with greater sensitivity, and can also search for rings around other trans-Neptunian dwarf planets.

Continuing to observe and track objects that are faint, recently discovered, or known to be changing is of high importance. JWST observations will be important for continuing to track the evolving ring arcs of Neptune (de Pater et al., 2005), the progressively winding ripple patterns in the rings of Jupiter and Saturn that trace cometary impacts (Hedman et al., 2011; Showalter et al., 2011), and other faint targets. It may also be capable of tracking the

azimuthal arcs or clumps in the rings of Jupiter (Showalter et al., 2007) and the "propeller" moons embedded in Saturn's rings (Tiscareno et al., 2010).

Spectroscopy of faint objects

The compositional diversity of solid objects in the outer Solar System is apparent from the near-infrared spectra of bodies such as Triton, Pluto and Charon, which show absorption features of varying strengths due to varying amounts of methane, water and other ices on their surfaces. The smaller moons and rings of Neptune might have originally been made of the same stuff as these larger objects, but they also would have had much different evolutionary histories (perhaps less thermal processing, more pollution from infalling matter, etc.). Comparing the surface composition of these smaller objects to their larger neighbors should therefore help clarify the origins and histories of both, but it is difficult to obtain good-quality spectra of these very small and/or faint objects from ground-based observatories.

With its large mirror and high-quality spectrometer, JWST will be able to take spectra of very faint objects. Potential targets include the rings and small moons of Uranus and Neptune; these have never been the subjects of high-fidelity spectroscopic study, as Voyager 2 did not carry a spectrometer capable of detecting them. Characterizing their chemical compositions is of considerable interest for addressing the origins of the Uranus and Neptune systems as well as for addressing the question of why the Uranian and Neptunian rings are so qualitatively different from those of Saturn (Tiscareno, 2013).

By the same token, JWST will be able to acquire very sensitive spectra of all objects over a broad range of wavelengths. It will be able to fill in the gap between Cassini VIMS and Cassini CIRS (from 5 to 8 μm) and will be able to map Saturn's rings in the 1.65- μm water absorption feature (which falls in an internal gap in VIMS' spectral coverage, and is unusual in that its depth is useful for mapping temperature variations). Its spatial resolution will be comparable to CIRS, and its sensitivity will be greater, so it should be capable of improving current maps of Saturn's rings in the thermal infrared (though over a very limited range of phase angles) and may achieve the first detection of the faint silicate absorption features at 10 μm, yielding information about the little-understood non-water-ice components of Jupiter's and Saturn's rings.

Equinox

The next Saturn equinox will take place in 2025. The event itself will not be observable by JWST, as it will occur when Saturn is near the Sun as seen from Earth, but low sun angles will be observable approximately three months before and after equinox. This will facilitate the observation of seasonal phenomena such as spokes, which are prevalent near equinox and absent near solstice (Mitchell et al., 2006, 2013). JWST will have sufficient resolution to continue monitoring spokes, as has HST (McGhee et al., 2005), which will have particular value after the end of the Cassini mission. JWST will also be able to improve on the tracking of clumps in and around the F Ring near equinox (McGhee et al., 2001), and will enjoy optimal edge-on viewing of Saturn's dusty rings during this season (de Pater et al., 1996, 2004). (The Phoebe ring, which lies in Saturn's orbit plane and is always edge-on as seen from Earth, is thus always available for optimal edge-on viewing.)

Neither Uranus nor Neptune has an equinox that falls within the JWST mission (Meeus, 1997). During the JWST mission, Sun angles will decrease at Neptune (solstice 1997, equinox 2038), and will increase at Uranus (equinox 2007, solstice 2030). This will lead to increasingly favorable viewing for both ring systems as the JWST mission progresses, since Neptune's rings are primarily dusty while Uranus' rings are dense and sharp-edged. The only exact equinoxes possibly observable by JWST will be at Jupiter; these will provide optimal viewing of vertical structure in the halo/gossamer rings.

Primitive Bodies

The small objects in the Solar System (e.g., asteroids, comets, and trans-Neptunian objects) will be of particular interest for study with JWST. This follows because they are thought to be 'primitive', preserving information about processes and chemistry in the solar nebula, and from the fact that many of them are too faint to have been studied in detail from the ground at near- to mid-IR wavelengths. The sensitivity of JWST will allow for compositional characterization of objects much smaller and further away, and with very high data quality. The modest spectral resolution of the instruments is well matched to studying the solid surfaces of these airless bodies, and will be useful for performing compositional studies of the gas comae of comets. These statements also apply at mid-IR wavelengths, but MIRI will additionally allow for the determination of albedos, diameters and thermal properties of a wide range of objects previously too faint to have such measurements. The trojan asteroids, centaur objects and irregular satellites of the planets also fall into this category.

Comets

Comets provide important clues to the processes that occurred during the formation and early evolution of the Solar System. In addition to their significant inventories of volatiles, they have orbits with aphelia in the outer Solar System, which are unstable due to perturbations by the giant planets. These properties suggest that comets are objects that have resided in the outer Solar System since the time of planetesimal formation and have only recently been perturbed onto orbits entering the inner Solar System. The degree of devolatilization and thermal processing must vary between comets, but as a class they represent packages of relatively pristine material which are uniquely suited to study because they come close to the Earth and Sun, and their outgassing provides the opportunity to determine the composition of materials in their interiors. Past observations, as well as laboratory measurements of cometary material obtained from the Stardust mission, suggest that comets contain a mixture of both interstellar and nebular material. A major observational challenge in cometary science is to quantify the extent to which individual comets, or parts of comets, can be linked to either reservoir.

JWST will support studies of many aspects of comets and their behavior, including being able to track even relatively fast-moving targets. Imaging will provide information on nuclear composition, diameter, albedo and thermo-physical properties. Regarding the dust coma, imaging will also enable investigation of the production rate and distribution; jet activity; activity evolution; and the dust temperature, albedo, and emissivity. Because JWST will offer such a huge improvement in spatial resolution in the mid-IR, near-nucleus processes in the dust coma may be particularly amenable to study via imaging. Imaging will also provide some compositional information regarding cometary nuclei and dust, particularly for small and/or distant objects and those with very small dust production rates. The available filters should allow discrimination of various silicate components and the identification of water and other ices.

JWST will support compositional studies of cometary nuclei, gas and dust with unprecedented sensitivity throughout the 1-30 μm range via the various spectroscopic modes. These data will allow determination of the composition, grain-size and temperature of dust in the coma and of the nucleus. The spectral resolution of the JWST instruments is not high enough to support all studies of cometary gases that can be done from the ground, but will provide very high sensitivity and spatial resolution, as well as access to wavelengths that can't be observed from the ground.

Figure 14 and Figure 15 give illustrative examples of the thermal emission from 29P/Schwassman-Wachmann 1 observed using Spitzer in the MIRI wavelength regime. These can be compared to the sensitivity of MIRI, illustrated in Figure 16 and Figure 17. The nucleus of 29P/S-W 1 has a diameter of about 25 km and was observed at heliocentric distance of about 6 AU. The coma optical depth was estimated as 10^{-9}, with a production rate less than 50 kg/s.

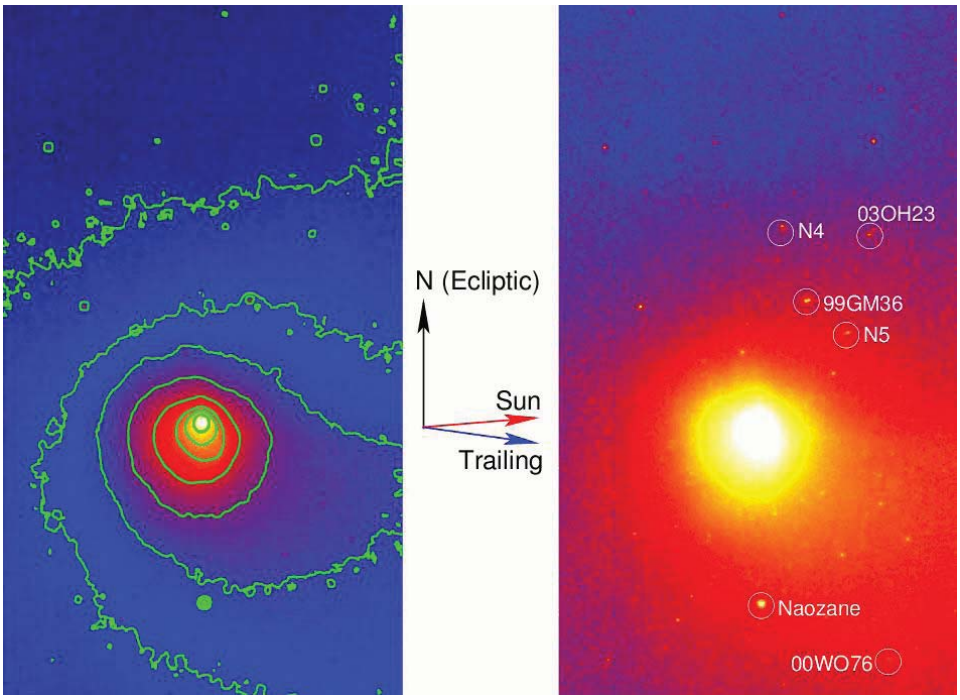

Figure 14. Map of the 24-μm emission from comet 29P/Schwassmann-Wachmann 1 made using the MIPS instrument on Spitzer Space Telescope (from Stansberry et al., 2004). MIRI will be considerably more sensitive than MIPS was, but has a much smaller field of view (these maps, which are two representations of the same data, are 17′ across).

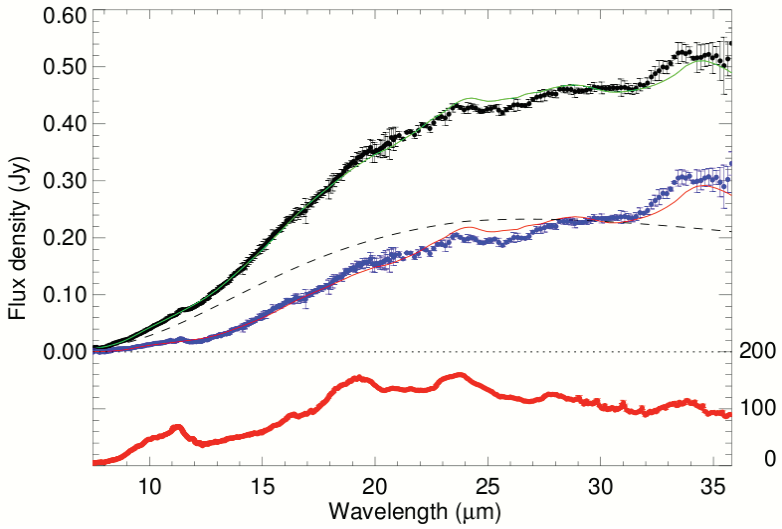

Figure 15. The emission spectrum of comet 29P/Schwassmann-Wachmann 1 (top panel) made using the MIPS instrument on Spitzer Space Telescope (from Stansberry et al., 2004) compared to the ISO spectrum of comet Hale-Bopp (lower panel; Crovisier et al. 1997). The 29P spectra are as measured (black points) and after removal (blue) of a model of the thermal emission from the nucleus (black dashed line). Note that 29P was more than 100 times fainter than Hale-Bopp.

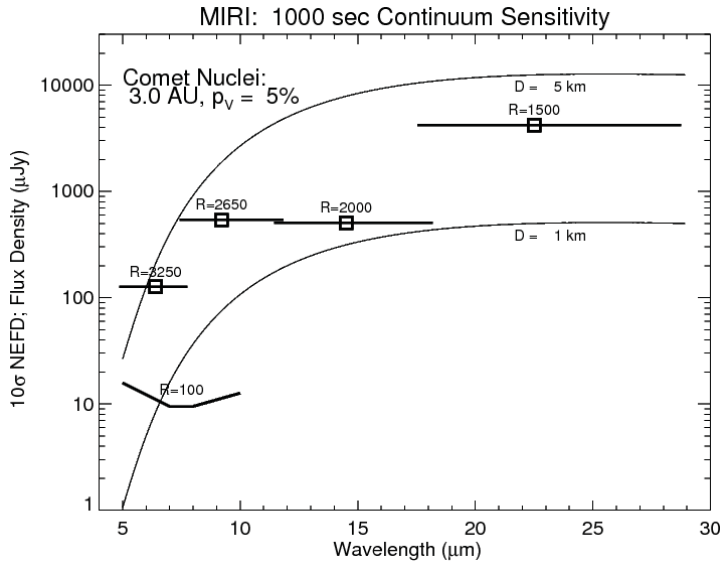

Figure 16. The sensitivity of MIRI low-resolution spectroscopy compared to models of the thermal emission from comet nuclei at 3 AU, where coma emission is typically negligible.

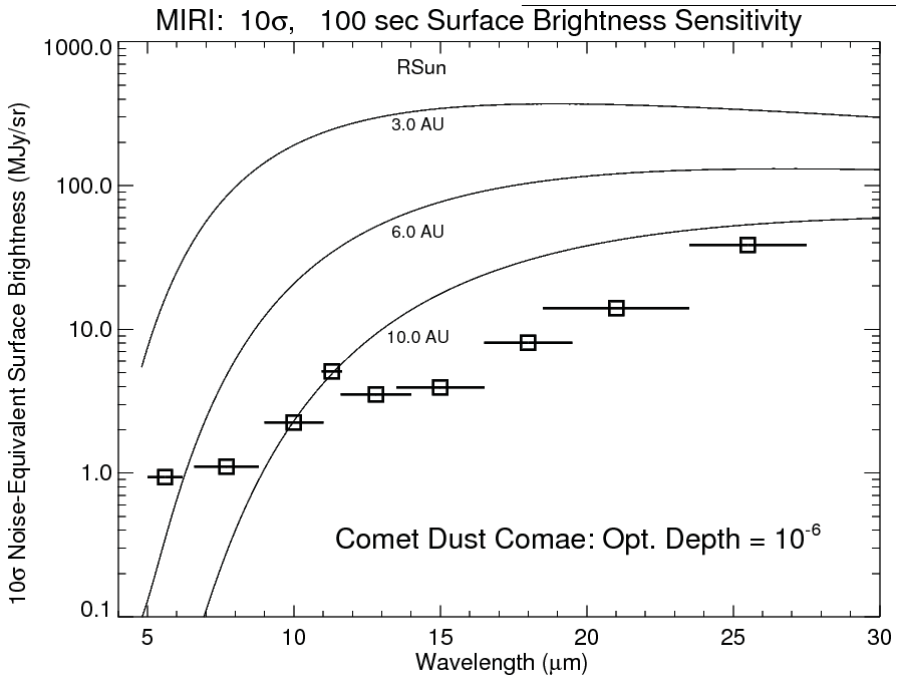

Figure 17. MIRI per-pixel sensitivity to extended emissions is compared to models of emission from coma dust at a range of distances from the Sun. The dust optical depth is assumed to be 10^{-6} in all cases. MIRI will provide outstanding capabilities for detecting and mapping the dusty comae of relatively active comets at high spatial resolution. Pixels may have to be binned to detect emission such as that shown in Figure 14, resulting in lower spatial resolution but high sensitivity.

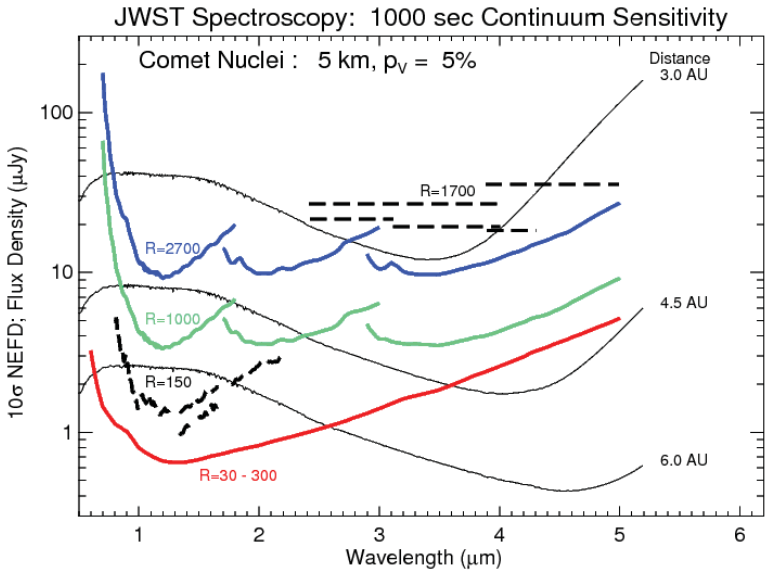

Figure 18. JWST spectral sensitivity (noise-equivalent flux density, or NEFD) curves compared to models of reflected plus emitted spectra for comet nuclei. The sensitivity curves are for a 1000-second exposure and a signal-to-noise ratio of 10. Thick solid lines are for NIRSpec at spectral resolving powers $30 < R < 300$ (prism), 1000, and 2700. Thick dashed lines are for the NIRISS R=150 slitless grism (paired with several different bandpass filters) and for the slitless NIRCam R=1700 slitless grism, also paired with available bandpass filters. The thin curves are the model spectral distributions for comets at different distances from the Sun and JWST (assumed equal). Objects are assumed to be spectrally neutral with a visual geometric albedo of 5%, and 5 km in diameter.

MIRI LRS data from 5-14 μm will be sensitive to the emission features of silicates, PAHs and other large organic molecules. The LRS data also provides sensitive constraints on the temperature of the dust, and grain size distribution. The LRS data will only be taken on the near-nucleus region of the coma. MIRI can also be employed to collect 10-μm images of the coma and near-nucleus dust trail. The images will reveal jet structures in the coma, providing constraints on the rotation state of the nucleus; the dust production rate, and the velocity of ejection. Each comet would be observed twice to sample activity at different phases in its orbit.

NIRSpec will be capable of detailed characterization of the composition of comet nuclei, as shown in **Error! Reference source not found.**. The NIRCam and NIRISS grism modes could also be useful for studying small, distant comets, particularly if they are too faint, or have ephemeris uncertainties too large, to allow target acquisition to hit a NIRSpec slit.

As can be seen in Figure 19, NIRSpec medium resolution spectra will enable characterization of broad emission lines from H_2O, CO_2 and organic molecules in the gas phase. These spectra will also be highly sensitive to the presence of water ice and silicates in the dust grains of the coma. Spectra will be taken of the region surrounding the comet nucleus to characterize the gas and dust composition before interactions with UV and chemical evolution have taken place, and also at a position offset from the nucleus to characterize the photo/chemical processes in the coma. NIRSpec high resolution spectra will be used to measure abundances of higher-order organic molecules, as well as isotope ratios of some volatiles in comae.

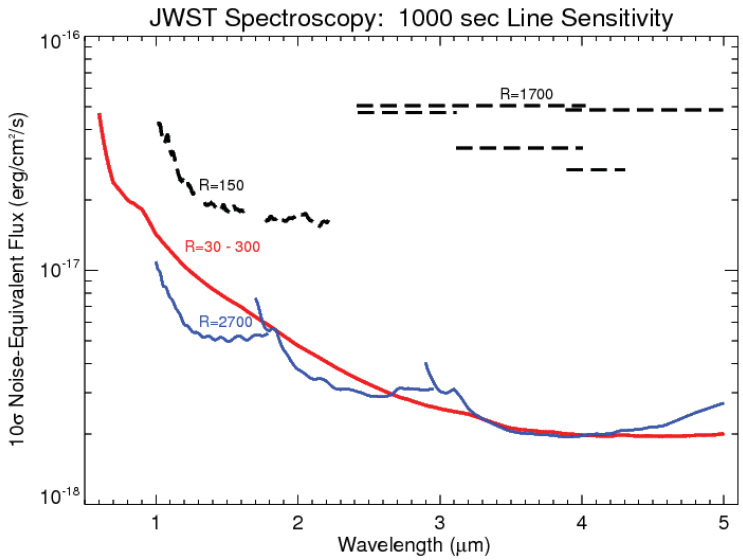

Figure 19. The sensitivity of NIRSpec to emission in unresolved lines. The NIRCam and NIRISS grisms are much less sensitive to such emission due to their lack of slits.

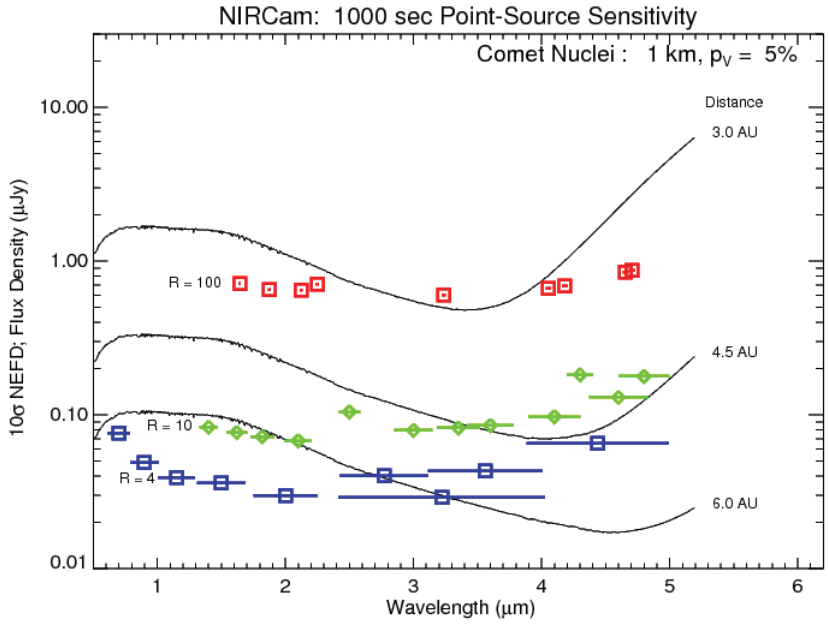

Figure 20. The sensitivity of NIRCam compared to models of reflected light plus thermal emission from small comet nuclei.

NIRCam and NIRISS could be used for characterizing the composition of faint comet nuclei via multi-filter imaging. Depending on the heliocentric distance, some of the emission could be thermal, complicating interpretation

of such data. Comets at distances beyond 6 AU should have almost no thermal emission shortward of 5 μm, and these instruments are sensitive enough to measure the near-IR colors of objects as small as 1 km using relatively short exposures.

Kuiper Belt Objects

JWST offers the possibility of vastly improving our understanding of the composition of objects in the trans-Neptunian region. These bodies, known as TNOs or Kuiper Belt Objects (KBOs), are thought to be planetesimals formed in the proto-solar disk and nebula and which never accreted to form planets. The KBO population does, however, include all but one of the five dwarf planets: Pluto, Eris, Haumea, and Makemake. The Kuiper belt and KBOs are in many ways similar to the asteroid belt and asteroids. Dynamically, the asteroid belt is influenced by various resonances with Jupiter, while the Kuiper belt was sculpted by the outward migration of Neptune. The asteroid belt contains many 'families' of objects, which formed via disruptive collisions; the Kuiper belt contains only one known collisional family, so far. On the other hand, the Kuiper belt does contain several dynamically distinct classes of objects that are not collisional families: the classical KBOs, with dynamically cold and dynamically hot subclasses (which differ by having low or high values of inclination); the resonant KBOs (of which Pluto is the archetype), the scattered KBOs (e.g., Eris and Sedna); and the centaurs, KBOs that have been recently perturbed onto non-resonant orbits with perihelia inside Neptune. The provenance and history of these dynamical classes are one of the key questions regarding the Kuiper belt.

The primary difference between the two populations is compositional, with the asteroids being dominated by silicates with significant admixtures of organics and metals. The KBOs are much more volatile rich, with large fractions of water but also other species such as nitrogen, methane, carbon monoxide and dioxide, although they too must contain significant amounts of silicates. The largest KBOs have densities of about 2 g/cm^3, consistent with about a 50:50 mix of silicates and water. Interestingly, the fifth dwarf planet, Ceres, which resides in the asteroid belt, has the same density as the KBO dwarf planets, suggesting that it is probably very water rich. The KBOs are thought to be volatile rich because they formed in the outer solar nebula and disk where such species were cold enough to condense. Because of this, studying the composition of KBOs should provide unique insights into both the volatile content of the early solar nebula, and into processes that operated in the outer parts of the nebula and disk during planet formation. The volatile species present on KBOs, as well as many organic compounds known or expected to exist on their surfaces, also happen to have their vibrational absorption bands in the near-IR where they are amenable to characterization with NIRCam, NIRSpec and NIRISS. Many silicate absorption/emission features are also present, some in the near-IR but also throughout the MIRI wavelengths. MIRI also will allow the determination of surface temperature distributions on KBOs, via modeling of the slope of their SEDs. This information is diagnostic of the thermal inertia and roughness of the surfaces, providing additional insights into the regolith properties of these objects. Those properties are, in turn, probably influenced by the collisional environment in the trans-Neptunian region.

The figures below illustrate the sensitivity of the JWST instruments in comparison to the reflected and emitted radiation from KBOs. Due to limits on the sensitivity of the ground-based instruments and observatories used to find KBOs and determine their orbits, the smallest known KBOs are probably about 50 km in diameter. A vast majority of the known population have diameters of 100 km or larger. JWST and its instruments offer such a quantum leap in sensitivity that it would be possible, in principle, to obtain high-quality near-IR multiband photometry for every known KBO. Additionally, many fundamental absorption features occur in the L and M bands, which are very difficult to observe at adequate sensitivity from the ground.

Using NIRCam it will be possible to obtain near-IR colors for a statistically significant sample of objects from each of the dynamical classes mentioned earlier, as illustrated in Figure 21. Because most KBOs are closer than 45 AU from the Sun (especially the smaller ones), the example shown is somewhat conservative. Such a data set would expand the existing near-IR colors for large TNOs and could form the basis of a spectral classification scheme, similar to that developed for asteroids, for the Kuiper Belt.

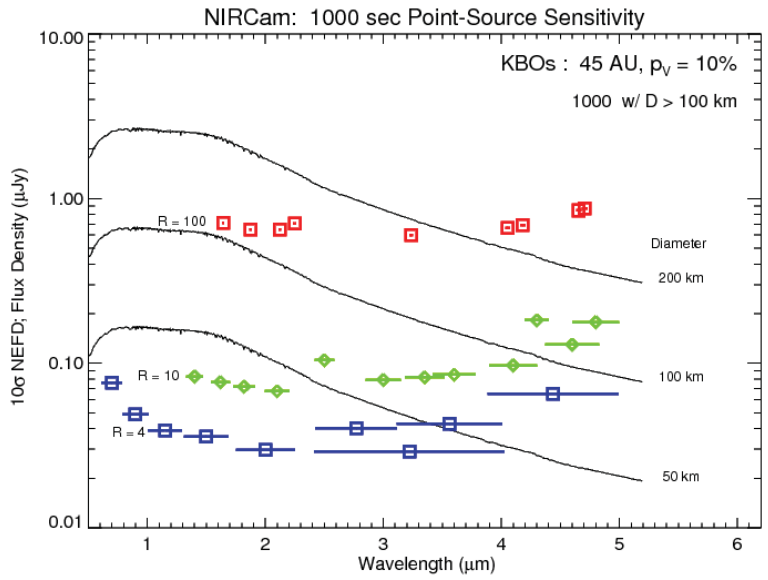

Figure 21. The sensitivity of NIRCam compared to model reflectance spectra for small KBOs (assumed to be spectrally neutral for this figure). The vast majority of the known KBOs could readily be observed at high-SNR using the NIRCam medium-band filters.

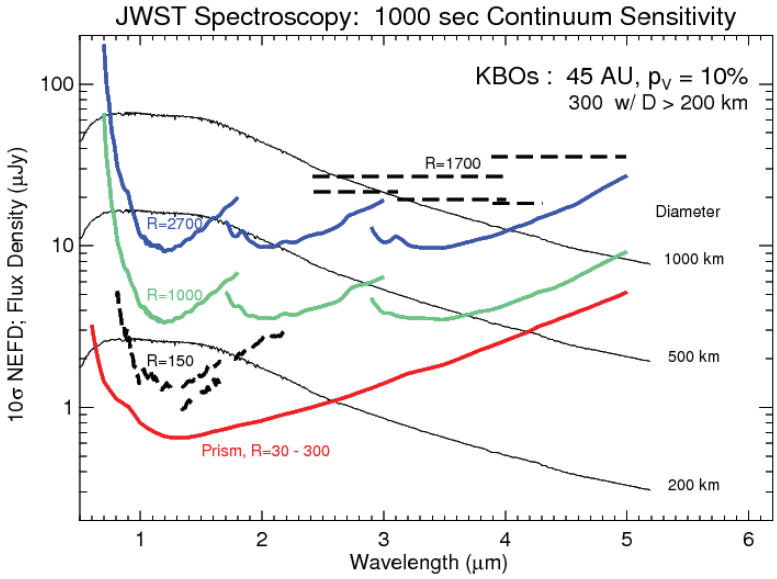

Figure 22. JWST spectral sensitivity (noise-equivalent flux density, or NEFD) curves compared to models of reflected plus emitted spectra for Kuiper Belt objects. The sensitivity curves are for a 1000-second exposure and a signal-to-noise ratio of 10. Thick solid lines are for NIRSpec at spectral resolving powers $30 < R < 300$ (prism), 1000, and 2700. Thick dashed lines are for the NIRISS R=150 slitless grism (paired with several different bandpass filters) and for the slitless NIRCam R=1700 slitless grism, also paired with available bandpass filters. The thin curves are the model spectral distributions for KBOs with a range of diameters. Objects are assumed to be spectrally neutral, with assumed visual geometric albedo of 10% and at 45 AU from the Sun and JWST (assumed equal).

NIRSpec will enable high-SNR spectral studies of a significant sample of KBOs, as illustrated in Figure 22. Using the prism, spectra could be obtained for even very faint/small objects, and would be highly diagnostic for water ice and some of the volatile ices (although only CO_2 would likely be retained on objects with diameters less than about 1000 km).

Using simple simulations of relatively short observations (three 970-s exposures) of KBOs with the NIRSpec IFU and at low spectral resolution (from 30 to 300 across the 0.6-5.0 μm range), we have computed a first order estimate of which fraction of water ice could be unambiguously detected as a function of the diameter of the object.

The results are shown in Figure 23. Even for small objects (diameters as small as 400-500 km), it is possible to detect the signature of water ice with a high level of confidence even for (geometrical) dilution factors of 10 (i.e. fraction of 10%). For reference, in our simple model, an object with a diameter of 500 km would have an H-band magnitude of typically 19-20 (see Figure 24).

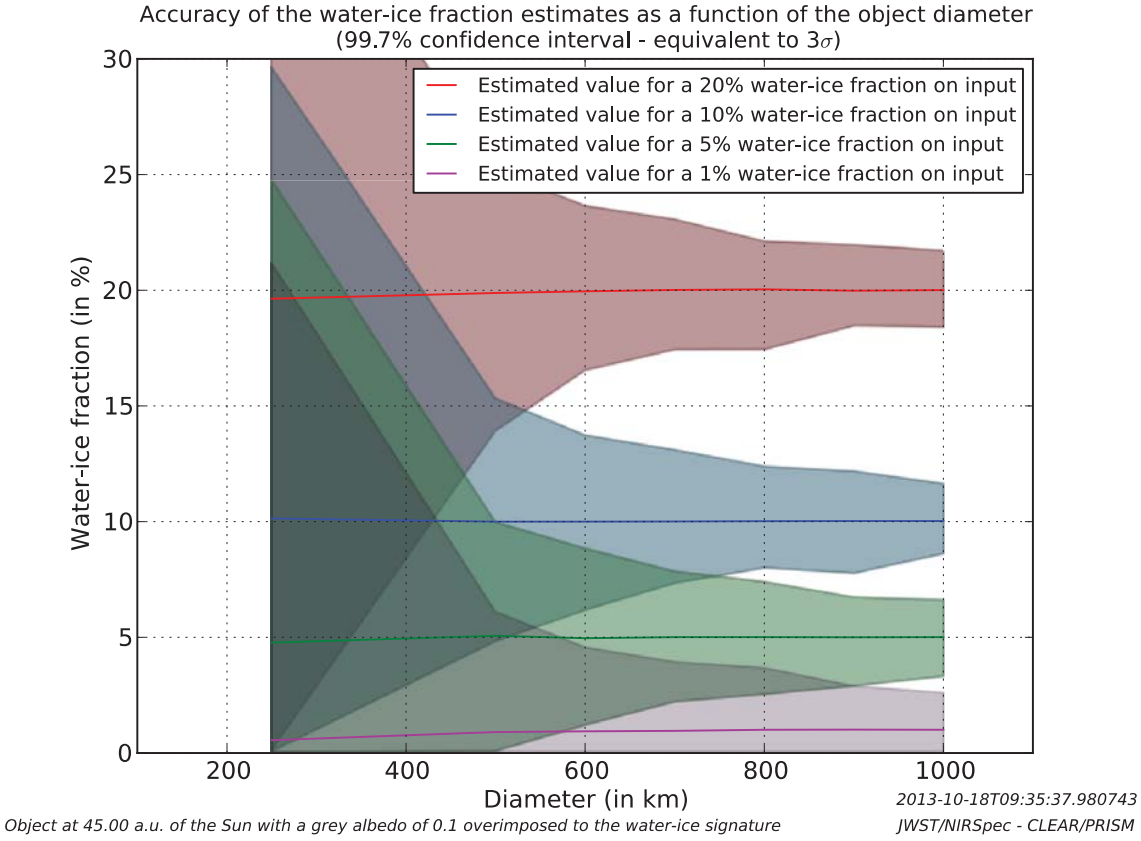

Figure 23. Accuracy of the water ice fraction estimates as a function of the object diameter and of the input water ice fraction. Simulations based on inputs from A. Guilbert-Lepoutre.

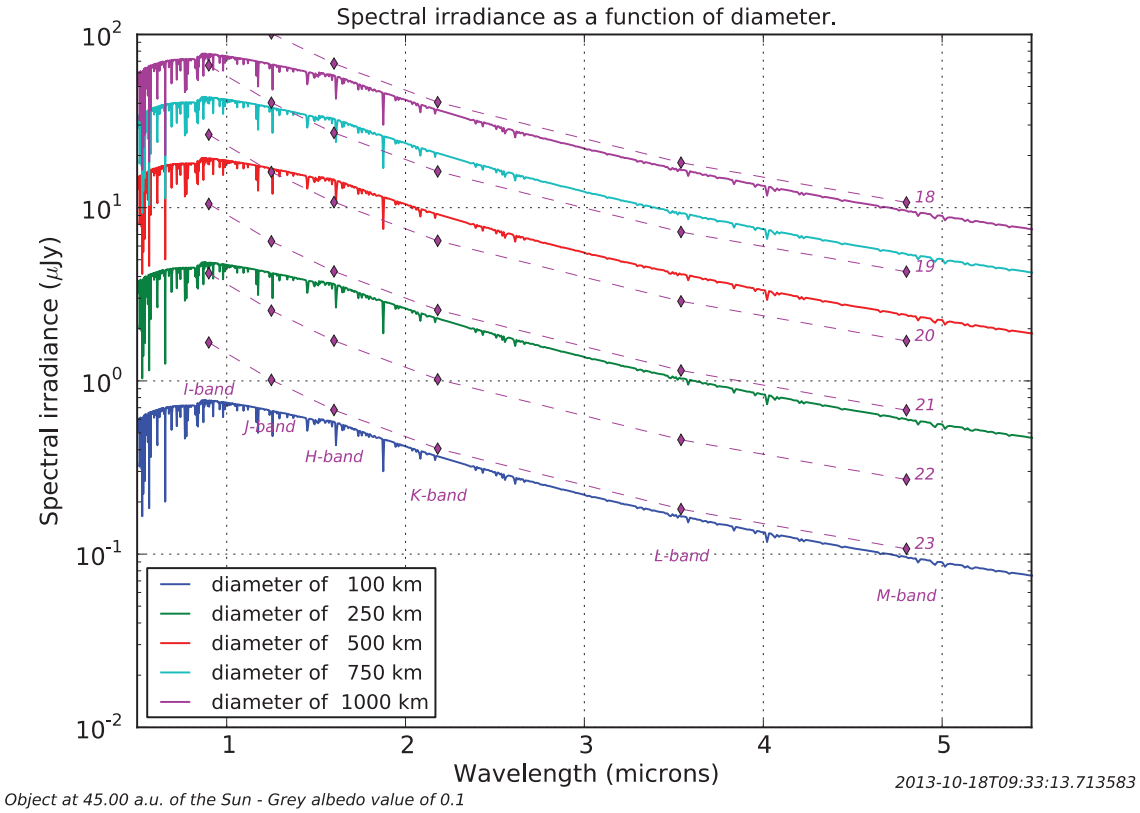

Figure 24. Figure showing the correspondence between the diameter of an object in our simple model and its observed magnitude in various bands. Simulations based on inputs from A. Guilbert-Lepoutre.

At *R*=1000 various hydrocarbon species can be easily detected, and those are stable against escape on most KBOs and are expected to be present. Such data would also be useful for characterizing volatile species such as CH_4, CO, CO_2 and N_2, but those ices probably only exist on the largest KBOs which are bright enough to be observed at high-SNR in *R*=2700 mode. Sedna is, perhaps, the exception because it is so distant and faint.

Figure 25 illustrates this more clearly, and shows the kinds of absorption features present in the spectra of the largest KBOs. Methane and water ices dominate the spectra, but other species are present albeit with weak and/or narrow absorptions. Silicates are commonly used to model the red visible slopes and spectral shapes near 1 μm and have been detected at 10 μm for at least one centaur object. High-order hydrocarbons similar to those seen in Titan's atmospheric hazes are also frequent components in such models, and are expected photolysis products when CH_4 and N_2 are present. Of the objects shown in Figure 25, only Pluto has a measured spectrum in the L and M bands. This illustrates just how difficult it is to observe KBOs in the near-IR from the ground: JWST has the sensitivity to revolutionize our understanding of KBO compositions by providing data in this poorly-explored but important spectral region.

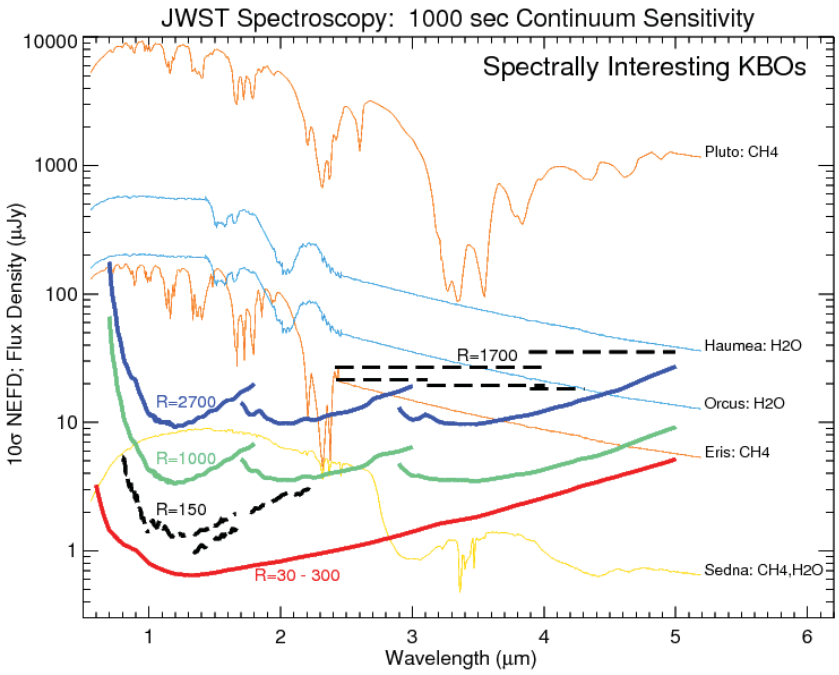

Figure 25. JWST spectral sensitivity (noise-equivalent flux density, or NEFD) curves compared to models of reflected plus emitted spectra for Kuiper Belt objects. The sensitivity curves are for a 1000-second exposure and a signal-to-noise ratio of 10. Thick solid lines are for NIRSpec at spectral resolving powers $30 < R < 300$ (prism), 1000, and 2700. Thick dashed lines are for the NIRISS R=150 slitless grism (paired with several different bandpass filters) and for the slitless NIRCam R=1700 slitless grism, also paired with available bandpass filters. The thin curves are the model spectral distributions for the indicated Kuiper Belt objects, with the dominant ice causing the absorptions noted for each. Other ices identified by weaker absorption features on KBOs are due to CO, CO_2, N_2, NH_3, and methanol (CH_3OH). The spectrum shown for Orcus is a scaled version of the Haumea spectrum. Spectra were furnished by D. Cruikshank (Pluto), F. Merlin (Eris), J. Emery (Sedna), and K. Barkume (Haumea). Model spectra were computed using observing circumstances estimated for mid-2019.

Another example of how NIRSpec could be used to distinguish between different ice compositions is shown in Figure 26. The "noisy" spectrum has been generated using a simple simulation of an observation of an Orcus-like object with NIRSpec in its IFU mode and at R=1000. In three exposures of 970 s, the signal-to-noise ratio in the spectrum is already high enough to have clear diagnostics on the ice composition.

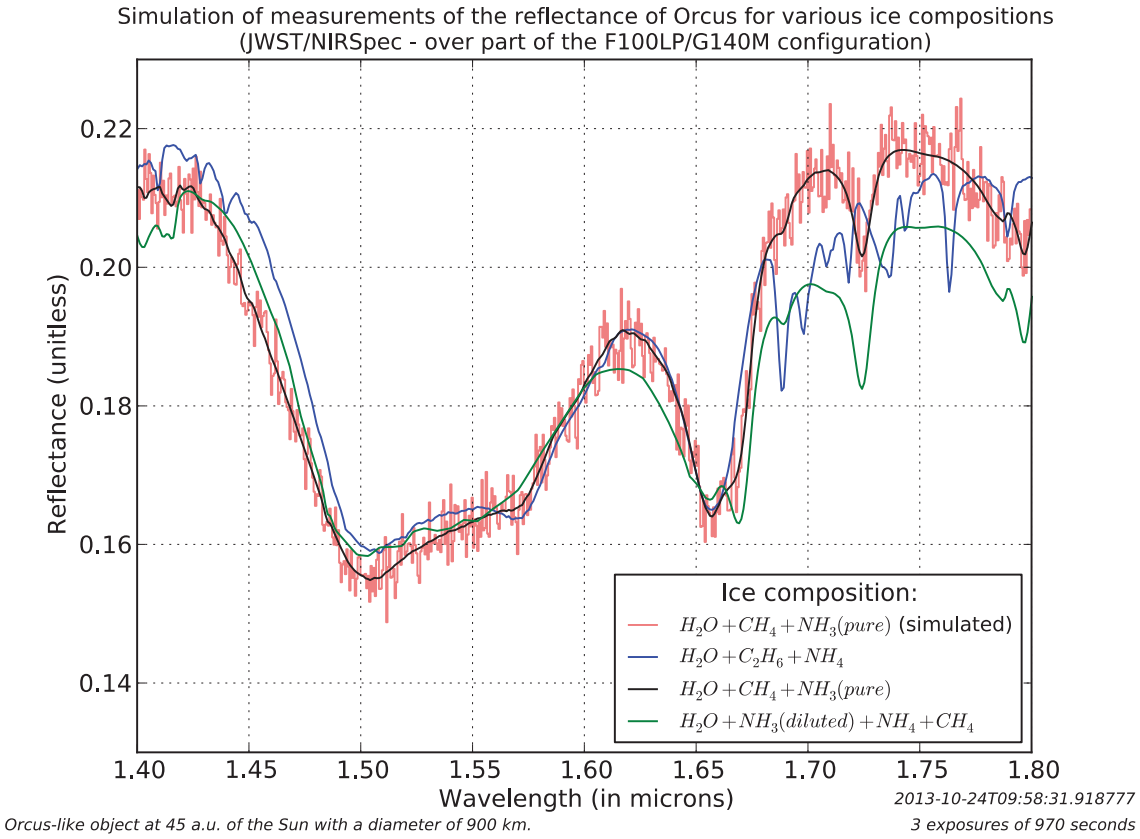

Figure 26. Results of a (simple) simulation of the measurement of the reflectance of an Orcus-like object with NIRSpec in its IFU mode and at medium spectral resolution (F100LP/G140M configuration). Shown here is the 1.4-1.8 µm wavelength range with the reflectance spectra of several different ice mixtures superimposed, including the mixture used as an input for the simulation. Data courtesy of A. Guilbert-Lepoutre.

MIRI will also allow characterization of KBOs, with reflected sunlight dominating the spectra shortward of about 12 µm and thermal emission dominating longward of that, as shown in Figure 27. Photometry at 7.7, 10, 11.3 and 12.8 µm could be diagnostic of silicate or PAH features. Photometry at 18, 21, and 25 µm is diagnostic of the temperature of the KBOs.

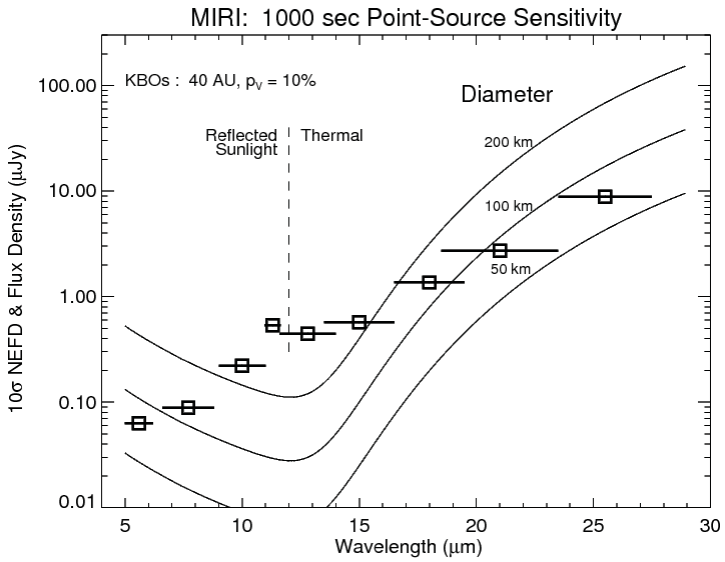

Figure 27. The sensitivity of MIRI imaging compared to model spectra for KBOs. Reflected sunlight dominates out to about 12 μm, while thermal emission is more important longward of that.

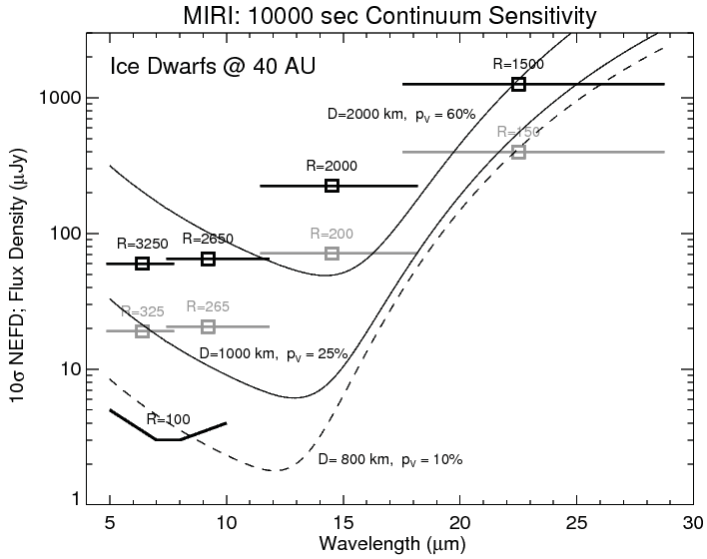

Figure 28. The sensitivity of MIRI spectroscopy is compared to model spectra for large KBOs. The sensitivities are plotted for the full resolution (values 1500-3250, plotted in black) and after binning to a resolution ten times lower (plotted in gray). Even with JWST, mid-IR spectra will only be possible for the largest objects.

Asteroids

Like the comets and KBOs, asteroids are remnants from accretion processes that occurred in the early phases of the formation of the Solar System. Unlike those bodies, asteroids formed inside the "snow-line" of the nebula, interior to which water was present as a gas rather than as ice. Because of that, asteroids are dominated by refractory compounds (silicates, metals, organics), although there is evidence for hydrated minerals (especially in the outer parts of the asteroid belt), and Ceres may contain a significant fraction of water ice in its interior. NIRSpec medium-resolution spectra in the 0.9-5 μm region will be used to search for organics, hydrated minerals, and water ice for a sample of ~100 small (D < 20 km) asteroids in the outer Main Belt (3.5-4 AU). Features from these materials will occur in the 1.5-5 μm region; spectra in the 0.9-1.5 μm region will constrain the silicate composition of each body so that a more accurate and complete picture can be drawn of the compositional diversity in general, and between families of asteroids. Current dynamical models for the evolution of the Solar System indicate that some asteroids (including Ceres) may have originated in the Kuiper belt; spectral studies may help in identifying objects with spectra similar to those of KBOs, and distinct from the larger population of asteroids.

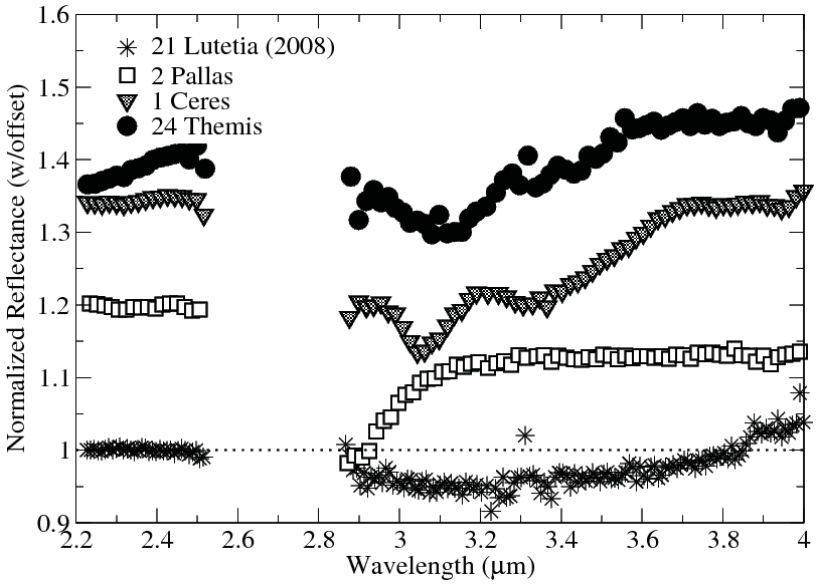

Figure 29. Reflectance spectra of asteroids in the 2-5 μm region display considerable diversity. Figure courtesy of A. Rivkin.

At MIRI wavelengths asteroid spectra are dominated by thermal emission. Photometric or spectroscopic measurements of that emission can be fit using thermal models to determine asteroid diameters, surface temperatures, albedos, and temperature distributions. Figure 31 illustrates this by giving example thermal-emission spectra for asteroids with a range of surface properties. Asteroids also exhibit spectral features in the mid-IR, produced by silicates such as olivine and pyroxene, and these can be readily detected in MIRI LRS spectra. Figure 31 illustrates the kinds of spectral features using emissivity spectra from three Jovian trojan asteroids as examples. Mid-IR data for Main Belt asteroids show similar features.

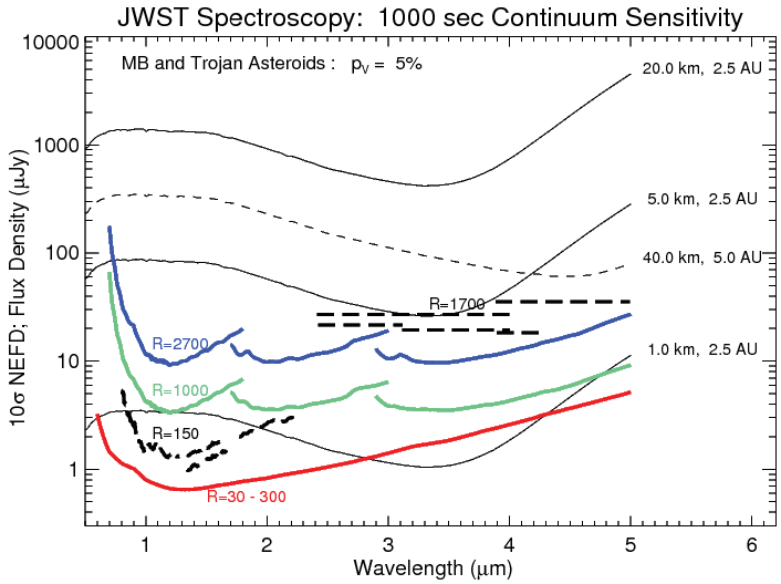

Figure 30. JWST spectral sensitivity (noise-equivalent flux density, or NEFD) curves compared to models of reflected plus emitted spectra for asteroids. The sensitivity curves are for a 1000-second exposure and a signal-to-noise ratio of 10. Thick solid lines are for NIRSpec at spectral resolving powers $30 < R < 300$ (prism), 1000, and 2700. Thick dashed lines are for the NIRISS R=150 slitless grism (paired with several different bandpass filters) and for the slitless NIRCam R=1700 slitless grism, also paired with available bandpass filters. The thin curves are the model spectral distributions for Main-Belt asteroids (solid lines) and a Jupiter Trojan (dashed line), at appropriate distances from the Sun and JWST (assumed equal). The assumed diameter for each object is given in the legend. Objects are assumed to be spectrally neutral, with a visual geometric albedo of 5%.

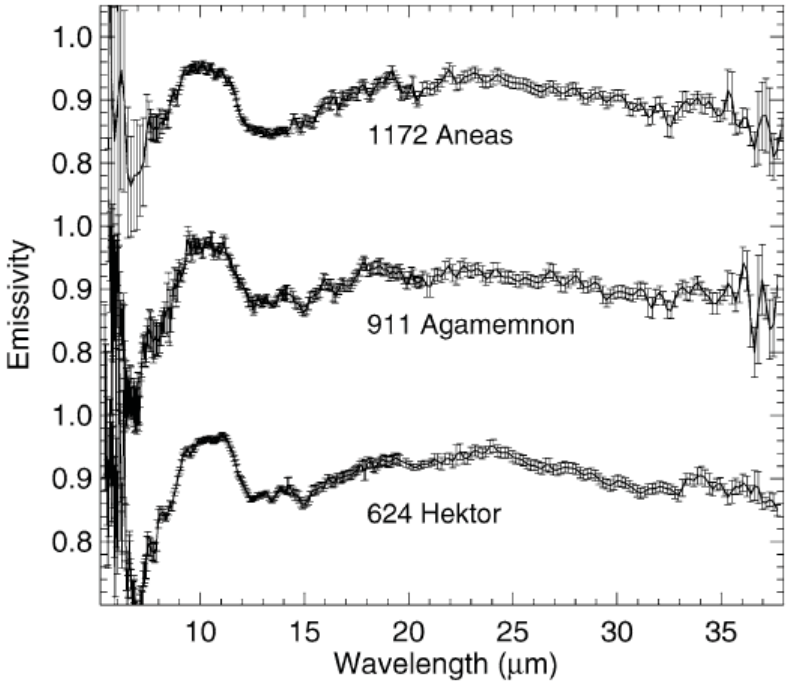

Figure 31. Emissivity spectra of three Jovian trojan asteroids obtained with the Spitzer IRS instrument. Emission features throughout the 5-30 μm range are attributed to silicates, and their presence requires that the surfaces of these objects be 'fluffy' and fine-grained.

MIRI LRS spectra of Main Belt asteroids will provide sensitive determination of the temperature distribution on their surfaces, as well as compositional information through the silicate emission features broadly clustered around 10 μm wavelength. The objects were selected to have similar sizes (as determined by IRAS), and are in two groups: high-albedo objects near 2.5 AU (S-type), and low-albedo objects near 3.5 AU (C-type). Each target will be observed twice in order to better constrain the thermal inertia of surface materials. For objects with large-amplitude (>0.25 mag) rotational lightcurves, the two observations will be timed to coincide with lightcurve minimum and maximum. For objects with smaller lightcurve amplitudes (0.1-0.2 mag), one observation will be timed to view the dawn-side emission, and a second later will view the dusk-side emission.

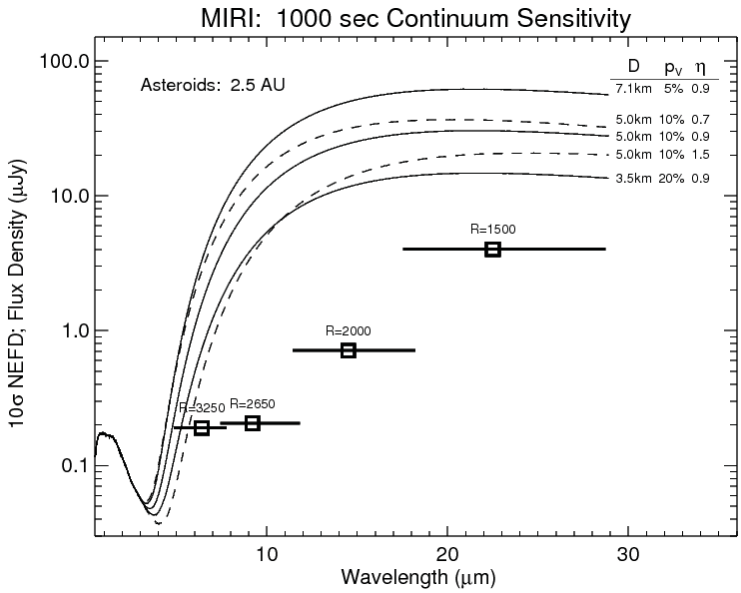

Figure 32. The sensitivity of MIRI spectroscopy at the highest available resolution is compared to model spectra for small Main Belt asteroids (assumed to be spectrally gray). The models are constructed in such a way that all five objects have the same brightness in the visible, but have different diameters, geometric albedos (p_V), and surface temperature distributions (as characterized by the beaming parameter η). MIRI spectroscopy and/or photometry of asteroids will allow characterization of their compositions and physical parameters at very high SNR.

Observations to complement other missions

JWST will also contribute observations that will complement data obtained from numerous spacecraft missions. While JWST cannot compete with the spatial resolution attainable with spacecraft visitations, its large platform has facilitated instrumentation with superior spectral resolution. Furthermore, the longer temporal baseline granted by JWST observations will greatly assist investigations of temporal variations of spacecraft targets, due to changes in season, heliocentric distance, solar activity, or internal processes.

Cassini

NIRSpec and MIRI provide improvements over Cassini's instrument package, offering greater spectral resolution (R=2300 and R=3000) than VIMS (R~200) and CIRS ($R \leq 2800$). This will allow a more precise identification and characterization of spectral features in the near and mid infrared. Additionally, MIRI will cover the 5-7 μm gap between the spectral coverage of VIMS and CIRS. Further details regarding JWST observations complementing the Cassini dataset are discussed in earlier sections.

Another important benefit of JWST observations will be more complete coverage of the Saturnian seasonal cycle. Cassini arrived at Saturn in mid-2004, just after southern solstice, and the mission will be terminated in 2017, near northern solstice. JWST will become operational soon afterwards, enabling views of the Saturnian system throughout most of the remaining half of the seasonal cycle: from northern solstice to southern solstice, as shown in Figure 33. A clear benefit will be investigation of the effects of changing sub-solar latitude upon Saturn's atmosphere, rings, and moons, especially to quantify any lag or asymmetry in the seasonal changes. Observing

campaigns will also benefit from changing views of the Saturnian system during JWST's lifetime, as different latitudes of Saturn and its moons become sunlit (and therefore visible).

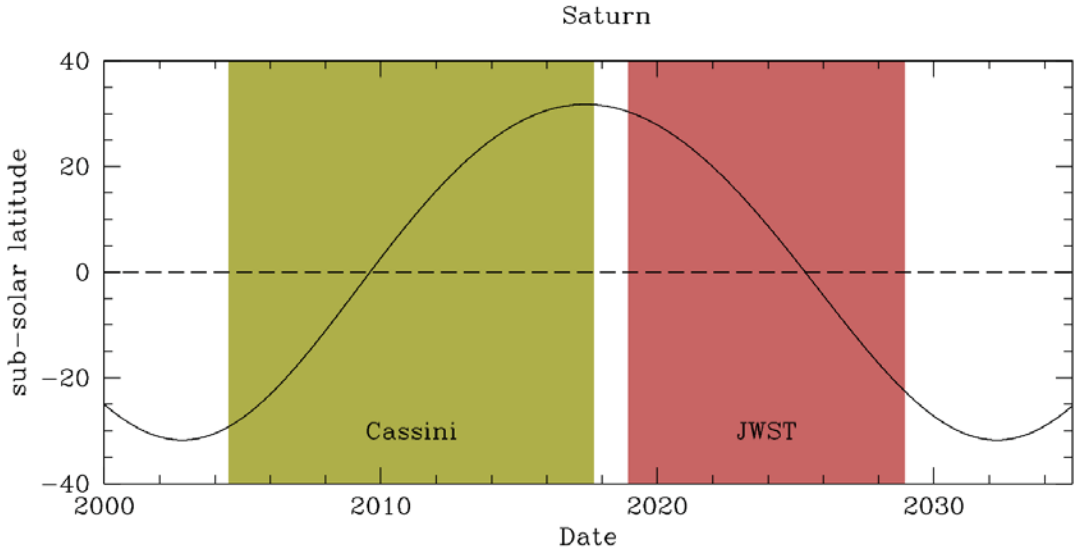

Figure 33. Saturn's sub-solar latitude during the period of JWST operations (red) compared to Cassini operations (gold).

Rosetta

ESA's Rosetta mission is designed to rendezvous with Jupiter-family comet 67P/Churyumov-Gerasimenko. It will arrive in mid-2014 when the comet is near 4 AU from the Sun and remain through the comet's August 2015 perihelion, ultimately ending operations in December 2015. As shown in Figure 34, JWST will be able to conduct follow-up observations during the comet's next two orbits.

Few limitations exist in JWST's ability to observe the comet. In previous apparitions, the comet's peak brightness has been V~12[3], so saturation will not be an issue. The comet's 2-km nucleus (Kelley et al. 2009) is also large enough to be observed near aphelion with NIRSpec (using moderate resolution) and MRS. The only issue will be the comet's speed: for a period near the comet's 2021 perihelion, it will be moving too fast for JWST to track.

[3] http://sci.esa.int/science-e/www/object/index.cfm?fobjectid=14615

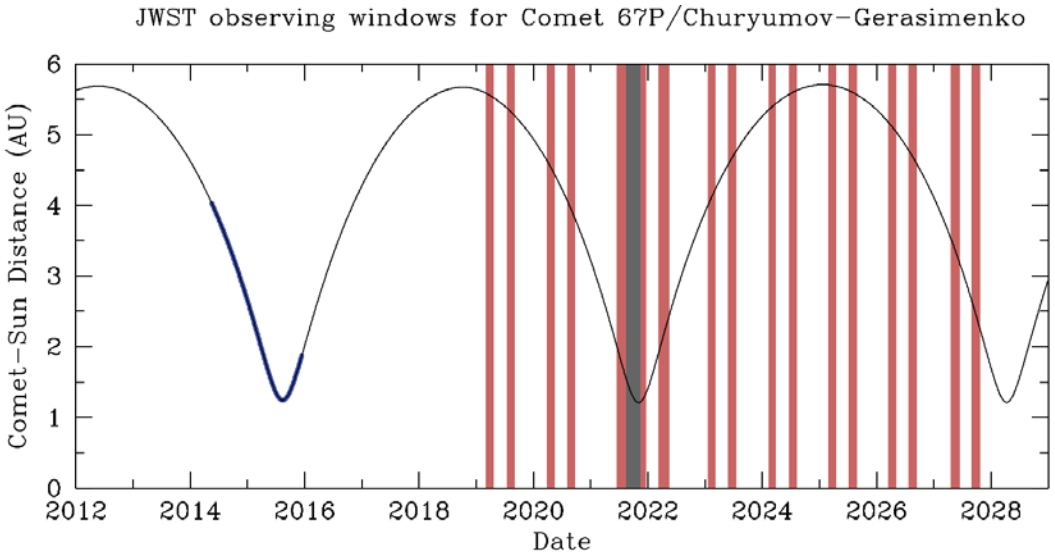

Figure 34. Observations of comet 67P/Churyumov-Gerasimenko compared to its heliocentric distance. Rosetta's 2014-2015 rendezvous with the comet is shown as a thick blue line. JWST observing windows are shown as solid red bars. The gray region--near the comet's 2021 perihelion--denotes where the comet is at a viewing angle observable with JWST, but is moving faster than JWST's maximum tracking rate of 0.03″ per second. The comet's 2028 perihelion occurs during a broad span where it is at an angle not observable with JWST.

Other missions

There are several other missions where seasonal changes are less important, but JWST will still be able to augment the observational dataset. None of the missions listed below have mid-infrared capabilities, and JWST will have much greater spectral resolution in the near infrared. Near- and mid-infrared observations of these mission targets with JWST will greatly assist in precise characterization of global surface properties of the spacecraft targets, as well as enable investigations of their thermal properties.

- NASA's Dawn mission, having orbited Vesta in 2011-2012, will arrive at Ceres in February 2015, with primary observations to last through July of that year. Other asteroid visitations with less-known schedules include OSIRIS-REx and the proposed Hayabusa 2 and MarcoPolo-R missions; the proposed targets of these three missions are all observable with JWST.

- NASA's New Horizons spacecraft will conduct its flyby of Pluto in July 2015, but will be observing Pluto for about five months beforehand as well. JWST observations will benefit studies of seasonal change on Pluto, which will experience solstice in 2029.

- The mission timespan for JWST (2018-2028) almost completely spans the interim between the Juno and JUICE missions, operated by NASA and ESA, respectively. Juno will be at Jupiter from July 2016 to October 2017. JUICE will reach Jupiter in January 2030 at the earliest, and will observe Jupiter and the three outer Galilean moons for almost three years before entering orbit around Ganymede.

Online resources

Below are links to JWST pages online. These pages are routinely updated with current information.

JWST design and instrument overview:

http://www.stsci.edu/jwst/overview/design/

Resources for Solar System observations with JWST:

http://www.stsci.edu/jwst/science/solar-system

PDF "pocket guides" for each instrument:

MIRI: http://www.stsci.edu/jwst/instruments/miri/docarchive/miri-pocket-guide.pdf

NIRCam: http://www.stsci.edu/jwst/instruments/nircam/docarchive/NIRCam-pocket-guide.pdf

NIRSpec: http://www.stsci.edu/jwst/instruments/nirspec/docarchive/NIRSpec-pocket-guide.pdf

NIRISS: http://www.stsci.edu/jwst/instruments/niriss/docarchive/NIRISS-pocket-guide.pdf

References

Aharonson et al. (2009). *Nature Geoscience* 2, 12, 851-854.

Baines et al. (2005), *Earth, Moon, and Planets* 96: 119-147.

Balzano and Zak (2006), Proc. SPIE 6274.

Carlson et al. (2009). In *Europa*, eds. Pappalardo et al., 283.

Castillo-Rogez and Turtle (2012). 44th DPS meeting.

Chen et al. (2010). JWST-STScI-001757: http://www.stsci.edu/jwst/instruments/miri/docarchive/

Chyba (2000). *Nature* 403, 6768, 381-382.

Crovisier et al. (1997). *Science* 275, 1904-1907.

de Pater et al. (2007). *Science* 317, 1888-1890.

de Pater et al. (2006). *Science* 312, 92-94.

de Pater et al. (2005). *Icarus* 174, 263-272.

de Pater et al. (2004). *Icarus* 172, 446-454.

de Pater et al. (1996). *Icarus* 121, 195-198.

Encrenaz et al. (1999) *P&SS* 47, 1225.

Farmer and Goldreich (2006). *Icarus* 180, 2, 403-411.

Fletcher et al. (2010). *A&A* 514, A17

Gaeman et al. (2012). *Icarus* 220, 2, 339-347.

Gardner et al. (2006) *Space Sci. Rev*. 123, 485-606.

Gerakines et al. (2000). *A&A* 357, 793-800.

Griffith et al. (2000). *Science* 290, 509-513.

Hand et al. (2007). *Icarus* 189, 2, 424-438.

Hand and Carlson (2011). *Icarus* 215, 1, 226-233.

Hedman et al. (2011). *Science* 332, 708-711.

Howett et al. (2012), *Icarus* 221, 2, 1084-1088.

Kelley et al. 2009, *AJ*, 137, 6, 4633-4642.

Kumar, et al. (2011). EPSC-DPS Joint Conference.

Lellouch et al. (2000). *P&SS* 48, 1393.

Lorenz et al. (2008). *Geophys. Res. Letters* 35 L02206.

Lunine et al. (2010): http://www.stsci.edu/jwst/doc-archive/white-papers

Lunine and Lorenz (2009). *Annual Review of Earth and Planetary Sciences* 37, 1, 299-320.

McCord et al. (1998). *Science* 280, 5367, 1242.

McGhee et al. (2005). *Icarus* 173, 508-521.

McGhee et al. (2001). *Icarus* 152, 282-315.

Meeus (1997). *Journal of the British Astronomical Association*, 107, 332.

Meier et al. (2000). *Icarus* 145, 462-473.

Meixner et al. (2008). JWST-STScI-001375: http://www.stsci.edu/jwst/doc-archive/technical-reports

Mitchell et al. (2013). *Icarus*, in press.

Mitchell et al. (2006). *Science* 311, 1587-1589.

Sanchez-Lavega (2011). *An Introduction to Planetary Atmospheres* (book).

Schaller et al. (2009). *Nature* 460, 7257, 873-875.

Showalter and Lissauer (2006). *Science* 311, 973-977.

Showalter et al. (2011). *Science* 322, 711-713.

Showalter et al. (2007). *Science* 318, 232-234.

Showalter et al. (2006). *Planet. Space Sci.* 54, 844-854.

Steffl and Stern (2007). *AJ* 133, 1485-1489.

Pappalardo et al. (1998). *Nature* 391, 365.

Pappalardo and Schubert (2013). 44th LPSC.

Stansberry et al. (2004). *ApJ* 154, 1, 463-468.

Tamayo et al. (2011). *Icarus* 215, 1, 260-278.

Tiscareno (2013). In *Planets, Stars, and Stellar Systems, Volume 3: Solar and Stellar Planetary Systems*, 309-376. (arXiv:1112.3305).

Tiscareno et al. (2010). *AJ Lett.* 718, L92-L96.

Turtle et al. (2011). *Science* 331, 1414-1417.

Webster, C.R. et al. 2013. Published online 19 September 2013 [DOI:10.1126/science.1242902].